Development and Validation of an Ambulatory Heart Rate Variability Measurement System

Olli Heikkinen

Master of Science Thesis
April 2011
Biomedical Engineering
Degree Programme on Science and Engineering
Department of Applied Physics
University of Eastern Finland
Kuopio

UNIVERSITY OF EASTERN FINLAND, Faculty of Science and Forestry
Department of Applied Physics
Degree Programme on Science and Engineering, Biomedical Engineering
HEIKKINEN OLLI PETTERI: Development and Validation of an Ambulatory Heart Rate Variability Measurement System
Master of Science thesis, 64 pages
Supervisors:
Mika Tarvainen, PhD, Docent
Jukka Lipponen, MSc
Olli Tikkanen, MSc
April 2011

Keywords: Ambulatory Biosignal Measurement, Heart Rate Variability, Electrocardiography, Bland-Altman Analysis, Welch's Periodogram, Autoregressive Spectrum Estimation, Least Squares Estimation, Smoothness Priors.

Introduction: Validation of measurement accuracy and precision of an electrocardiography (ECG) based ambulatory heart rate variability (HRV) measurement system (eMotion HRV by Mega Electronics) were assessed in laboratory and field conditions. Also, data acquisition software for the system was developed in this work in C# for Windows. HRV can be used to assess the control of the autonomic nervous system on the heart in e.g. cardiology, diabetes care and sports science.

Methods: The system was validated by simultaneous measurements with an MDD and FDA approved clinical ECG device. Orthostatic, bicycle ergometer and 24 h daily activity experiments were conducted on five healthy, young persons. The accuracy of QRS detection of the system was assessed with sensitivity and positive predictivity measures. Precision of measured ECG RR intervals in the laboratory experiments was assessed with histogram of RR differences and Bland-Altman analysis. The effect of the differences in RR intervals between systems was assessed by calculating a set of time domain and frequency domain HRV measures for both systems from the orthostatic experiment data. Spectrum estimation methods Welch's periodogram and stationary AR(16) model were used. Smoothness priors was implemented to detrend the data before spectrum analysis. Reliability of the system in long-term measurements was assessed with artefact ratio analysis. All analysis methods, a QRS detection algorithm and an artefact detection algorithm were implemented in Matlab.

Results: The sensitivity and positive predictivity were $s_{\mathrm{qrs}} = 99.989$ % and $p_{\mathrm{qrs}} = 99.989$ %. The 95 % limits of agreement from Bland-Altman analysis were (0.591 ± 0.962) ms during rest and (0.820 ± 1.308) ms during exercise. The smallest difference between systems in HRV measures was 0.001 % and the highest 0.718 %. The artefact ratios in the 24 h daily activity measurements were 0.009 % at the lowest and 0.266 % at the highest.

Conclusions: The eMotion HRV system was accurate in QRS detection and the differences between systems in measured RR intervals and calculated HRV measures were small. Thus, the performance of the system was comparable to the clinical ECG device in laboratory measurements and the quality of data was good also in long-term measurements in field conditions.

ITÄ-SUOMEN YLIOPISTO, Luonnontieteiden ja metsätieteiden tiedekunta
Sovelletun fysiikan laitos
Teknis-luonnontieteellinen koulutusohjelma, Lääketieteellinen tekniikka
HEIKKINEN OLLI PETTERI: Kannettavan sykevaihtelumittausjärjestelmän kehitys ja validointi
Pro Gradu -tutkielma, 64 sivua
Ohjaajat:
Mika Tarvainen, FT, Dosentti
Jukka Lipponen, FM
Olli Tikkanen, LitM
Huhtikuu 2011

Avainsanat: ambulatorinen biosignaalimittaus, sykevaihtelu, elektrokardiografia, Bland-Altman-analyysi, Welchin periodogrammi, autoregressiivinen spektriestimointi, pienimmän neliösumman menetelmä, Smoothness Priors.

Johdanto: Tässä työssä validoitiin elektrokardiografiaan (EKG) perustuvan kannettavan sykevaihtelumittausjärjestelmän ulkoinen ja sisäinen mittaustarkkuus laboratorio- ja kenttäolosuhteissa. Lisäksi työssä kehitettiin järjestelmälle datanpurkuohjelmisto C#-ohjelmointikielellä Windows-alustalle. Sykevaihtelua voidaan hyödyntää autonomisen hermoston sydäntä ohjaavien toimintojen tutkimuksessa muun muassa kardiologian, diabetologian ja urheilulääketieteen aloilla.

Menetelmät: Mittausjärjestelmä validoitiin vertailemalla sitä kliinisesti hyväksyttyyn EKG-mittausjärjestelmään yhtäaikaisten mittausten avulla. Validointimittauksia olivat ortostaattinen testi, rasitustesti ja vuorokauden mittainen pitkäaikaismittaus. Tutkimushenkilöinä oli viisi tervettä nuorta aikuista. Järjestelmän ulkoista tarkkuutta arvioitiin QRS-tunnistuksen erottelukyvyn ja positiivisten tulosten ennustuskyvyn avulla. Mitattujen RR-intervallien sisäistä tarkkuutta arvioitiin laboratoriokokeissa erotushistogrammin ja Bland-Altman-analyysin avulla. RR-intervallien erojen käytännön vaikutusta arvioitiin laskemalla ortostaattisen testin datasta molemmille järjestelmille joukko aika- ja taajuustason sykevaihteluparametrejä. Spektriestimointimenetelminä käytettiin Welchin periodogrammia, stationaarista AR(16)-mallia ja Smoothness Priors -trendinpoistomenetelmää. Järjestelmän luotettavuutta pitkäaikaismittauksissa arvioitiin artefaktasuhdeanalyysin avulla. Analyysimenetelmät ja algoritmit toteutettiin Matlab-ympäristössä.

Tulokset: Erottelukyky ja positiivinen ennustuskyky olivat $s_{\mathrm{qrs}} = 99.989$ % ja $p_{\mathrm{qrs}} = 99.989$ %. Bland-Altman analyysin tuloksina saadut 95 % luottamusvälit olivat (0.591 ± 0.962) ms levossa and (0.820 ± 1.308) ms rasituksessa. Sykevaihteluparametrien pienin ero järjestelmien välillä oli 0.001 % ja suurin 0.718 %. Vuorokausimittausten artefaktasuhde oli pienimmillään 0.009 % ja suurimmillaan 0.266 %.

Johtopäätökset: Järjestelmä oli ulkoisesti tarkka ja erot RR-intervalleissa ja lasketuissa parametreissä olivat pienet järjestelmien välillä. Järjestelmän suorituskyky oli siis verrattavissa kliiniseen EKG-järjestelmään laboratorio-olosuhteissa ja datan laatu oli hyvä myös pitkäaikaismittauksissa kenttäolosuhteissa.

Acknowledgements

This work was carried out jointly at the Department of Applied Physics in the Kuopio campus of the University of Eastern Finland and at Mega Electronics, Kuopio, Finland from 2009 to 2011. I would like to thank my supervisors in both establishments for their good advice during the planning, measurement, analysis and writing phases of this work. Thanks go also to all the teaching staff at the university for giving me a good example on the scientific mindset and for great education on physiology, physics, signal analysis and English. Thank you to all the people at Mega for the insight on software design and for providing a great place to work.

I would like to thank my parents, Paula and Matti, as well as my siblings, Esa, Sanna and Aki, for all their support and for giving me an example on working in general and on how to go on and to complete demanding tasks. I want to thank my friends for all the good times and for being themselves. The most thanks go to my love, Kirsi, for sharing everything and giving reason.

In Kuopio, April 2011

Olli Heikkinen

List of Notations

$\in$	Belongs to
$\forall$	For all
$\mathbb{N}$	Natural numbers
$\mathbb{R}$	Real numbers
$\|x\|$	Absolute value of x
$\|\|x\|\|$	Euclidean norm of x
x^T	Transpose of x
$\hat{x}$	Estimate or prediction of x
$< x, y >$	Inner product (i.e. dot product) of x and y
$\overline{x}$	Average of x
D_2	Second order difference matrix
e	Observation error vector
e_t	White noise
$E\{x\}$	Expected value of x
$E(z)$	Z-transform of e_t
f	Frequency
f_s	Sampling frequency
H	Observation matrix
$H(z)$	System function
i	Imaginary unit, $i = \sqrt{-1}$
I	Identity matrix
p	Order of an AR model
$p(x)$	Probability density function of x
p_{qrs}	Positive predictivity of a QRS detection algorithm
$P_x(f)$	Power spectrum of x
r_x	Autocorrelation of x
$R(H)$	Range of H
s_{qrs}	Sensitivity of a QRS detection algorithm
s	Trend component of the HRV time series
u	Detrended HRV time series
U	Energy of a window function
w_t	Window function
W	Width of a window function in number datapoints
x	Observation vector
$X(z)$	Z-transform of x_t
Δ	Difference
ϵ	Residual
θ	Parameter vector
λ	Smoothing parameter in smoothness priors
σ_x^2	Variance of x

List of Abbreviations

Ag-AgCl	Silver-Silver Chloride
AIC	Akaike Information Criterion
ANS	Autonomic Nervous System
API	Application Programming Interface
AR(p)	Autoregressive model of order p
AV	Atrioventricular
BPM	Beats Per Minute
DFT	Discrete Fourier Transform
ECG	Electrocardiogram, Electrocardiography
EMG	Electromyogram, Electromyography
FFT	Fast Fourier Transform
FPE	Final Prediction Error
HF	High Frequency band
HR	Heart Rate
HRV	Heart Rate Variability
IDE	Integrated Development Environment
LA	Left Arm electrode
LF	Low Frequency band
LoA	Limits of Agreement
LL	Left Leg electrode
MDL	Minimum Description Length
RA	Right Arm electrode
RL	Right Leg electrode (ground electrode)
RR	Time interval between successive electrocardiogram R waves
PVC	Premature Ventricular Contraction
PNS	Parasympathetic Nervous System
QRS	Electrocardiogram wave complex, containing the Q, R and S waves
RMSSD	Root Mean Square of Successive Differences
RSA	Respiratory Sinus Arrythmia
SA	Sinoatrial
SDNN	Standard Deviation of Normal-to-Normal Beats
SNS	Sympathetic Nervous System
TINN	Triangular Interpolation of Normal-to-Normal interval histogram
ULF	Ultra Low Frequency band
VLF	Very Low Frequency band

Chapter 1

Introduction

Heart Rate Variability (HRV) analysis is a field of research with increasing popularity that has many viable applications in e.g. cardiology [8], diabetes care [6], sports science [26] and generally research on the autonomic nervous system , see e.g. [10]. The current clinical applications of HRV analysis include prediction of mortality risk after myocardial infarction and diagnosis of cardiovascular autonomic neuropathy [6, 38].

To facilitate the transition of HRV analysis from research to biomedical applications, there is a need to be able to measure HRV reliably for extended periods of time. Ease of measurement and reliable devices and algorithms for e.g. QRS detection are similarily of paramount importance for the success of HRV analysis in different applications.

In this thesis, a commercial HRV measurement system for long-term ambulatory measurements is introduced and validated. The system consists of a small one channel ambulatory electrocardiograph, a device-computer-interface and data acquisition software. The development of the data acquisition software was a part of this work, and thus, the design and implementation of the software are described in this thesis.

Concerning validation, the aims of this work are to assess the accuracy and precision of the measurement data produced by the system via comparison to the data produced by a golden standard system in resting and exercise conditions. Secondly, the effect of the differences in the data will be assessed by computing several well known HRV measures in time and frequency domain and comparing the measures between systems. Thirdly, the applicability of the measurement system to 24 hour daily activity measurements will be assessed utilising qualitative analysis of a diary of activities and an artefact detection algorithm developed in this work.

The second chapter of this thesis contains a brief review of the anatomy and physiology behind HRV. In the third chapter, measurement methods of HRV are assessed, while the fourth chapter is about analysis of HRV. The fifth chapter contains a description of the two measurement systems used in this thesis and in the sixth chapter, the measurement and analysis methods selected for this work are described. In the seventh chapter, the results of the validation experiments are shown and discussed and the eighth chapter concludes the thesis.

Chapter 2

Origin of Heart Rate Variability

The rhythm of the heart varies involuntarily from beat to beat as it adapts to changes in the surrounding environment. This adaption takes place to ensure adequate perfusion in vital organs in all situations. The oscillation can be assessed with a time series consisting of the time intervals between consecutive heart beats. The heart beat occurrence time is usually quantified with the peak of the R wave of the electrocardiogram (ECG) (see Section 3.1). This time series is called heart rate variability (HRV) [5].

Historically, the term "heart rate variability" has been understood to describe both the variation in the interbeat interval as well as in the instantaneous heart rate (the latter being the reciprocal of the former). Also, other terms describing the interbeat oscillation have been introduced: cycle length variability, heart period variability, RR variability [38]. To mitigate this inconsistency, only the most established term heart rate variability will be used in this thesis.

When assessing the validity of a biosignal measurement system, it is imperative to know the biological target of the measurement and the characteristics of the measurable signal. Therefore, in this chapter, a brief review of the human heart, the bioelectrical phenomena behind beating of the heart, the regulation of heart rate by the autonomic nervous system (ANS) and the periodic components of HRV is given. If not mentioned otherwise, the references for this chapter are [5, 12, 13, 22, 32].

2.1 The Human Heart

The heart is the centre of the circulation system feeding the whole body with oxygen and nutrients as well as participating in thermoregulation. The heart is located inside the ribcage, between the lungs and above the diaphragm. It weighs about 250-300 g and its longest axis is tilted, with the apex of the heart pointing downwards, usually a bit to the front from the coronal plane and left from the sagittal plane (see Figure 2.1a). The pumping of the heart and changes in posture alter the geometry and the position of the heart with respect to other organs during normal function.

The heart is essentially a large muscle, composed of specialised striated muscle cells. The cardiac muscle cells are connected to adjacent cardiac muscle cells via special gap junctions, which allow the rapid conduction of electrical signals between

cells. The voluntary contraction of the cardiac muscle is based on sliding overlapping actin and myosin filaments, which is powered by chemical energy bound to adenosine triphosphate molecules.

The cardiac muscle is divided into four separate hollow compartments: two atria and two ventricles (see 2.1a). The walls of the ventricles are substantially thicker than the walls of the atria. In addition, the left ventricle has a thicker wall than the right ventricle, thus it can produce the highest contraction force.

The atria and the ventricles are separated from each other by heart valves which open at appropriate times to allow blood flow from the atria to the ventricles. Blood enters the heart through the atria and exits through the ventricles. The contraction of different parts of the cardiac muscle in a cyclic, orderly fashion allows circulation of the blood in the correct directions.

During diastole, the resting phase of the heart, oxygenated blood from the lungs flows to the left atrium and at the same time deoxygenated blood from the peripheral circulation enters the right atrium through the superior and inferior vena cavae. After this atrial filling, both atria contract and pump the blood into the ventricles. During the subsequent contraction phase, systole, the ventricles contract and force the blood out 1) from the left atrium through the aorta to the peripheral circulation and 2) from the right ventricle through the pulmonary arteries to the lungs.

2.2 Cardiac Action Potential

The phenomenon that initiates the contraction of the cardiac muscle, is called the cardiac action potential. It is a bioelectrical event in which the voltage over the outer membrane of a nerve or a muscle cell (sometimes called the membrane potential) rises and falls back to the baseline. The shape of the action potential differs between different parts of the heart (for an example, see Figure 2.2).

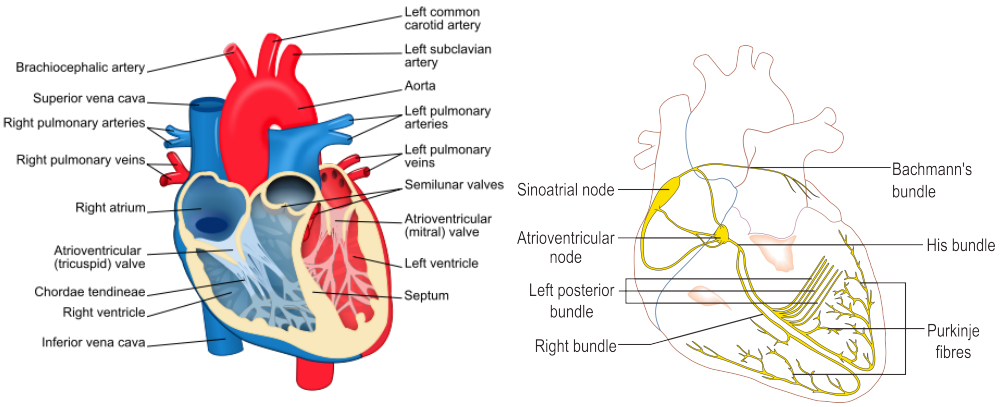

Figure 2.1: a) The heart. b) The conduction system of the heart.

Generation of Cardiac Action Potentials

Cardiac action potentials can be generated in certain parts of the conduction system of the heart, a network of specialised cardiac muscle cells (see Figure 2.1b). The primary source of cardiac action potentials is the sinoatrial node (SA node), the "pacemaker" of the heart, which is located in the upper part of the right atrium. When isolated from any nervous input, a healthy SA node generates action potentials with a rate depending on the age of the person. This intrinsic heart rate has been estimated to be $181.1 - (0.57 \times \text{age})$ beats-per-minute (BPM). In addition to the intrinsic heart rate, input from the autonomic nervous system to the SA node affects the actual rate at which cardiac action potentials are generated.

If the SA node does not function properly, or if there is a blockage in the conduction tract, another part of the conduction system can take the pacemaker role, e.g. the atrioventricular node (AV node) or even the Purkinje fibers. Without input from the upper parts of the conduction system, the AV node and the Purkinje fibers pulsate at their own intrinsic pulsation frequency, which is lower than the intrinsic heart rate. This limits the heart rate and therefore the performance of the heart.

Heartbeats that are not originated from the SA node are broadly called ectopic beats. One type of ectopy is a premature ventricular contraction (PVC), where the ventricles contract abnormally early and where the origin of the beat is in the AV node, in the atrium or in the ventricular muscle. PVCs cause very noticable distortions to the cardiac action potential seen in the electrocardiogram.

Intracellular Conduction of Cardiac Action Potentials

The conduction of a cardiac action potential inside a cardiac muscle cell is based on the active transportation and passive permeation of electrically charged ions through the cell membrane. At rest, the ionic distribution over the cardiac muscle cell membrane is anisotropic. There is an excess of potassium (K^+) ions inside the cell and a surplus of sodium (Na^+), calcium (Ca^{2+}) and chloride (Cl^-) ions outside the cell. This distribution makes the membrane electrically polarised, with the potential inside of the cell about 90 mV less than the potential outside. Osmosis force would balance the concentration differences over the membrane, but the imbalance is maintained by specialised ion-pumps, the Na^+-K^+ pump and the Na^+-Ca^{2+} pump.

In addition to the active ion-pumps, there are passive voltage sensitive ion channels in the cell membrane. These channels open when an action potential wave comes to their proximity e.g. from another cell. This allows the free flow of nearby ions into and out of the cell to decrease the concentration gradients over the membrane. Ion channels specific to Na^+ are fast to react to a voltage change, while the channels specific to Cl^-, Ca^{2+} and K^+ are slower.

The first phase of the cardiac action potential is depolarisation, where the Na^+ ions flow into the cell, increasing the membrane voltage quickly from a negative value to a positive one. The Na^+ channels close very rapidly and the second phase, repolarisation, begins with the opening of Cl^- channels, allowing Cl^- ions to flow into the cell. The following simultaneous opening of K^+ and Ca^{2+} channels induce

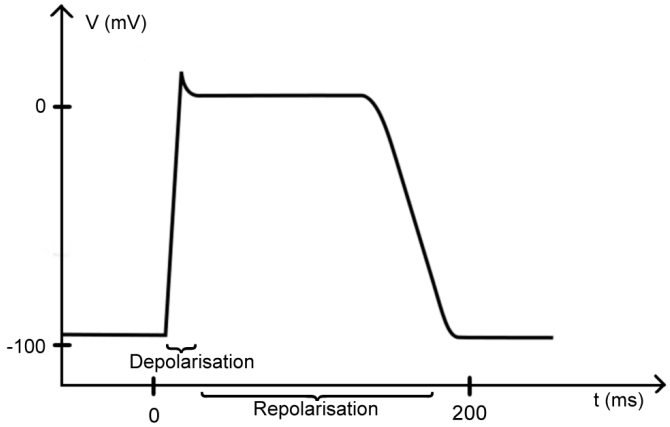

Figure 2.2: The action potential of a ventricular cardiac muscle cell.

a plateau in the membrane voltage. Finally, the flow of K^+ ions outside decreases the membrane voltage back to resting voltage (see Figure 2.2).

The Ca^{2+} ions now inside the cell initiate the contraction of the cardiac muscle cell. Because electrical charge flows through the aforementioned ion channels, also nearby ion channels, being sensitive to voltage changes, are triggered to open, therefore continuing the chain reaction of a moving action potential wave.

Intercellular Conduction of Cardiac Action Potentials

The action potential spreads to adjacent cardiac muscle cells efficiently via gap junctions, because they allow movement of the electrically charged ions between adjacent cells. The action potential generated in the SA node travels in two directions: The first target is the atrioventricular node (AV node), which lies between the atria and the ventricles, through three internodal tracts while simultaneously depolarising the cardiac muscle cells in the right atrium. The second target is the Bachmann bundle in the left atrium and depolarisation of the left atrium.

The conduction velocity of the action potential wave decreases significantly in the AV node. This provides an adequate temporal window for the contraction of the atria to drive the blood into the ventricles. There is an electrically insulating fibrous tissue layer between the atria and the ventricles, which does not allow the action potentials to move directly from the atrial cells to the ventricular cells.

After the significant delay in the AV node, the action potential wave moves rapidly through the His bundle, into the left and right bundle branches, and on into the Purkinje fibers, which spread the depolarisation wave to the ventricles. As the ventricles depolarise, the atria repolarise simultaneously. After a significant delay, the ventricles repolarise also, completing the contraction cycle of the heart.

2.3 Regulation of Heart Rate by the Autonomic Nervous System

Neurohumoral regulation of the function of the heart takes place to ensure adequate blood supply in vital organs. Neural regulation is performed by the autonomic nervous system (ANS) in an automatic and unconscious manner. The ANS can be physiologically divided into the sympathetic and the parasympathetic (also known as vagal) branches. The sympathetic nervous system is dominantly responsible for regulation of organs in activities associated with stress responses, which generally require a higher heart rate. The parasympathetic nervous system, on the other hand, has a dominant role in activities associated with rest, for which a slower heart rate is adequate.

Signal transfer in the nerves operates by conduction of action potentials; to a great extent in the same way as in ventricular muscle cells. The nerves consist of bundles of sequential neurons connected to each other by synapses. Notable deviations from the action potential of a ventricular muscle cell are shorter repolarisation time and the lower number of ions involved: only Na^+ and K^+ ions participate in the process. In addition, the conduction of action potentials in nerves is unidirectional because of the synaptic connections between individual neurons.

Because of the unidirectionality, both branches of ANS must have separate nerves for afferent signaling (sensory nerves) and efferent signaling (e.g. motor nerves). Afferent signals from the sensory receptor organs can be thought of as input to the heart rate control system in the brainstem, while the output from that system is the efferent signaling to e.g. the SA node.

Efferent Innervation

In the heart, the efferent nerves control e.g. the conduction velocity of cardiac action potentials, myocardial contractility, the diameter of coronary arteries and the heart rate (i.e. cardiac chronotropic control). The heart rate is regulated by direct sympathetic and parasympathetic innervation of the SA node and the AV node. Increased activity of the sympathetic efferent nerves and decreased activity of the parasympathetic efferent nerves stimulate the pacemakers, thus increasing the heart rate. Respectively, decreased sympathetic activity and increased parasympathetic activity inhibite the nodes, which decreases the heart rate.

Afferent Innervation

There are afferent nerve receptors in the heart, arteries, lungs and skeletal muscles that participate in regulation of heart rate. Baroreceptors in the walls of the atria, the ventricles, the aorta and the carotid arteries sense changes in blood pressure. Chemoreceptors, which can sense the concentration of oxygen and carbon dioxide in blood as well as pH and temperature of blood, can be found e.g. in the walls of the ventricles and in the common carotid artery.

The receptors of afferent parasympathetic and sympathetic nerves are in differ-

ent locations in the heart: The receptors of sympathetic afferent neurons are located in the epicardium, the outer part of the heart, while the parasympathetic afferent neurons synapse deeper in the heart, in the endocardium. This may expose the parasympathetic receptors to damage in ischemic heart disease associated necrosis of the endocardium.

Central Nervous System Connections

The ANS and its sensory organs also have connections to the central nervous system. Afferent signals from the heart, arteries, lungs, skin and skeletal muscles are transferred to e.g. the cortex and the hypothalamus, which in their own part affect the regulation of heart rate. The efferent connections downwards from the central nervous system allow also emotions and stress to have input on control of heart rate.

2.4 Periodic Components of Heart Rate Variability

By studying the temporal oscillations in the heart rate, it is in some cases possible to obtain indirect information about the normal function of the autonomic nervous system as well as discover novel diagnosis and therapeutic methods for neuropathologies. Also, by examining the interdependencies between HRV and other biosignals, e.g. blood pressure and respiration, it is possible to gain further insight into the autonomic nervous system.

Generally, the response of sympathetic nerve receptors to a stimulus is slow, in the order of seconds, while the response of parasympathetic receptors can be either slow or fast. Therefore, sympathetic nervous system activity causes low frequency oscillations in HRV, while the parasympathetic nervous system drives both lower and higher frequencies. To assess the periodic components of HRV more precisely, the spectrum of the signal and specific spectral bands can be studied. The most established division of the HRV spectrum is the following spectral bands [36, 38]:

- Ultra Low Frequencies (ULF): [0, 0.003] Hz
- Very Low Frequencies (VLF): [0.003, 0.04] Hz
- Low Frequencies (LF): [0.04, 0.15] Hz
- High Frequencies (HF): [0.15, 0.4] Hz

Some extensively studied phenomena appear on specific frequencies or frequency bands of HRV: The first relationship with HRV and another physiological process, respiratory sinus arrythmia (RSA), was observed already in the 18th century. In RSA, the heart rate accelerates during inhalation and decelerates during exhalation. The resulting frequencies in the HRV time series correlate are usually in the HF frequency band. Apart from RSA, the HF band oscillations are believed to be caused by parasympathetic activity.

The LF frequency band contains information about baroreceptor activity and the 0.1 Hz Mayer wave, which is caused by cardiac mechanoreceptors and chemoreceptors. It is generally believed that LF frequencies are the product of both sympathetic and parasympathetic activity.

The meaning of oscillations in the VLF and ULF frequency bands are less well defined. They could possibly be caused by changes in the renin-angiotensin system, thermoregulation, vasomotorics and also by humoral factors. In general, the system regulating the heart rate is very complex and more research is required to understand it entirely.

Chapter 3

Measurement of Heart Rate Variability

HRV is defined as a biosignal which is constructed from the time differences between consecutive heart beats, i.e. heart beat intervals. HRV is typically derived from the electrocardiogram (ECG), although it can also be reliably derived from magnetocardiography also [40, 41]. While magnetocardiography is an accurate bioelectromagnetic measurement method and requires no contact between the measurement devices and the subject, it is not suitable for ambulatory measurements.

Somewhat similar time series describing the cardiac cycle can be constructed from photoplethysmography, biomedical ultrasound, nuclear medicine, microwave reflectometry [27] and continuous blood pressure measurements. As these measurements yield information about circulation of blood or dimensions of the cardiac muscle, as opposed to the bioelectrical information obtained from ECG, they have different applications than HRV derived from ECG.

3.1 Electrocardiography

Electrocardiography (ECG), invented by Willem Einthoven in 1902 [9], is concerned with the measurement and analysis of the electrocardiogram (similarily abbreviated ECG), which is the electrical manifestation of the contractile activity of the heart. In other words, the ECG shows the voltage over time induced on the measurement electrodes by the cardiac action potential wave travelling through the heart. Measurement electrodes are usually placed on the surface of the thorax or on the limbs. ECG is used widely in the clinical as well as in the research laboratory setting e.g. to

- study the rhythm of the heart and to diagnose arrhythmias
- monitor the long-term effects of cardiovascular drugs
- diagnose conduction disturbances in the heart
- study metabolism and oxygen supply of the heart
- locate and measure injuries and scar tissue in the heart muscle
- assess overgrowth of the heart muscle
- diagnose electrolyte abnormalities
- assess cardiovascular risk in occupational and sports science [17, 22].

As the cardiac action potential (see Subsection 2.2) moves through the conduction system of the heart and activates contraction of the cardiac muscle cells, it generates a time-dependent electric field around the heart.

As defined in [22], the depolarisation and repolarisation waves of cardiac muscle contraction can be modeled as dipole layers, i.e. planes consisting of closely packed electrical dipoles normal to the plane surface. The dipoles in the layer model the extracellular potential caused by the influx and efflux of the electrically charged ions through the cell membrane.

When an approximately cylinder shaped cardiac muscle cell depolarises in one end (let us call this the activation origin), the extracellular potential at that end becomes negative (see Subsection 2.2). The easily conducting gap junctions between the cells force the emerging electrical field to be parallel to the cell. Thus, the emerging electrical field around the cell points away from the activation origin towards the other end, the activation target, which has positive potential around it. This can also be seen as a dipole with the negative end pointing to the activation origin and the positive end pointing to the activation target. Thus, the positive polarity of the dipole layer modeling the moving depolarisation wave is in the direction of wave movement. The negative polarity of the dipole layer points backwards.

Repolarisation wave follows the depolarisation wave with a delay dependent on the type of the cell [22]. The dipole layer modeling the repolarisation wave has reverse polarity compared to the depolarisation wave. Thus, the negative polarity points in the direction of movement of the wave and positive polarity points backwards.

If the voltage, caused by the movement of the dipole layers from the activation origin to the activation target, would be measured parallel to the cardiac muscle cell, with the ground electrode at the activation origin end, the voltage would be positive during the depolarisation, negative during the repolarisation and zero otherwise. This measurement can be called the electrogram [12, 13]. The electrocardiogram, on the other hand, is the sum of the electrograms produced by all the muscle cells in the heart.

3.1.1 Waveform of the Electrocardiogram

The waveform of the normal ECG signal from a healthy person during one cardiac cycle can be seen in the Figure 3.1. This form can be obtained from a measurement made parallel to the electrical axis of the heart, i.e. approximately parallel to the left and right bundle branches (see Figure 2.1b) with the ground electrode near the right clavicle and the positive electrode under the heart on the left side of the chest.

The normal ECG waveform consists of several waves, known as P, Q, R, S, T and U waves. The positive P wave is the result of depolarization of the atria. The baseline between the P and Q waves, the PQ interval, results from the delay of the depolarisation wave in the AV node. The repolarisation of the atria and the depolarisation of the ventricles occurs during the negative Q, positive R and negative S wave, together known as the QRS complex. Because of the larger muscle mass of the ventricles, ventricular depolarisation masks the repolarisation of the atria in the ECG. Thus, the QRS complex represents ventricular contraction [13, 22].

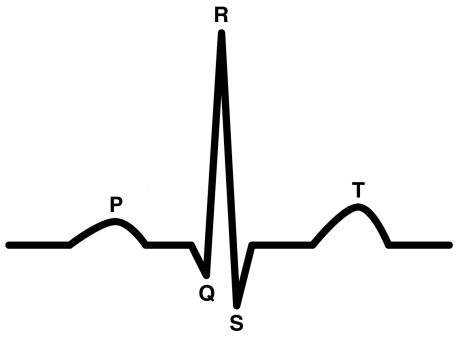

Figure 3.1: The waveform of the ECG with the different waves.

The T wave is caused by ventricular repolarisation. According to the description of the electrogram in the previous subsection, the repolarisation waveform on the ECG should be negative. But because the action potential duration in epicardium is shorter than in the endocardium, the epicardium repolarises before the endocardium, in spite of earlier depolarisation of the endocardium. Therefore the wave representing ventrical repolarization, the T wave, is positive [13, 22].

The shape and number of the waves can change due to cardiac pathologies [13, 22]. This is the basis for many cardiac disease diagnostics.

The frequency content of the ECG waveform lies between frequencies 0.05 and 500 Hz, while most of diagnostically relevant signal power is under 100 Hz. The QRS complex has center frequency around 17 Hz and the T wave a frequency of 1–2 Hz [17, 39].

3.1.2 Resting ECG

There are several different paradigms of ECG measurement for different purposes. Resting ECG is the most standard measurement paradigm in the clinical setting [17]. It utilises the international standard "12 lead ECG", in which 12 separate channels of ECG are measured by ten electrodes placed on the thorax and on the limbs. In ECG lexicon, the word "lead" can mean both a measurement channel and an electrode, thus the use of terms "channel" and "electrode" is preferred in this work.

Placement of the thorax electrodes in resting 12 channel ECG is the following [17] (see also Figure 3.2):

- V1 in the fourth intercostal space, at the right sternal border
- V2 in the fourth intercostal space, at the left sternal border
- V4 in the fifth intercostal space, in the left midclavicular line
- V3 between V2 and V4
- V6 in the left midaxillary line, at the horizontal level of V4
- V5 between V4 and V6.

Additionally, three limb electrodes are placed on the left wrist (left arm electrode, LA), on the right wrist (right arm electrode, RA) and on the left ankle (left leg

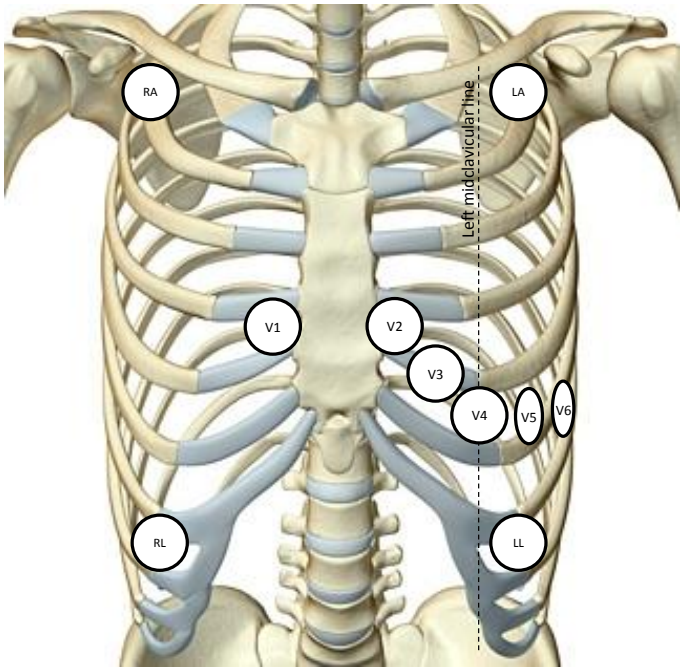

Figure 3.2: The locations of the thorax electrodes in the 12 channel ECG and the locations of the limb electrodes in the Masor-Likar modification [24].

electrode, LL). A ground electrode is placed on the right ankle (right leg electrode, RL).

The twelve ECG channels are bipolar measurements measured between two electrodes, using the right foot ground electrode as the reference. Let us denote the voltage between each electrode and the ground with LA, RA, LL, V1, V2, V3, V4, V5 and V6, respectively. Now the twelve bipolar ECG channels can be derived from these voltages:

$$\begin{aligned} \mathrm{I} &= \mathrm{LA} - \mathrm{RA} & \mathrm{V}_1 &= \mathrm{V1} - \mathrm{V_W} \\ \mathrm{II} &= \mathrm{LL} - \mathrm{RA} & \mathrm{V}_2 &= \mathrm{V2} - \mathrm{V_W} \\ \mathrm{III} &= \mathrm{LL} - \mathrm{LA} & \mathrm{V}_3 &= \mathrm{V3} - \mathrm{V_W} \\ \mathrm{aVR} &= \mathrm{RA} - \frac{1}{2}(\mathrm{LA} + \mathrm{LL}) & \mathrm{V}_4 &= \mathrm{V4} - \mathrm{V_W} \\ \mathrm{aVL} &= \mathrm{LA} - \frac{1}{2}(\mathrm{RA} + \mathrm{LL}) & \mathrm{V}_5 &= \mathrm{V5} - \mathrm{V_W} \\ \mathrm{aVF} &= \mathrm{LL} - \frac{1}{2}(\mathrm{RA} + \mathrm{LA}) & \mathrm{V}_6 &= \mathrm{V6} - \mathrm{V_W}, \end{aligned}$$

where $\mathrm{V_W} = \frac{1}{3}(\mathrm{RA} + \mathrm{LA} + \mathrm{LL})$ is the Wilson's Central Terminal, the average voltage of the three limb electrodes. The precordial channels V_1, V_2, V_3, V_4, V_5 and V_6, are written here with subscript to differentiate them from the above mentioned voltages.

3.1.3 Exercise ECG

In exercise ECG, a modified version of the resting ECG 12 channel system is often used. In this so called Mason-Likar electrode placement system [24], the thorax electrodes are placed in the same way as in resting ECG, but the limb electrodes are placed on the torso as shown in Figure 3.2. This reduces EMG artefact from muscles of the moving limbs and motion artefact caused by the moving electrode cables, but the alternate electrode placement may also somewhat distort the shape of ECG signal. Therefore, the exercise ECG measurements are not directly comparable with resting ECG measurements for all purposes [17].

3.1.4 Long Term ECG

Long term ECG monitoring is used for arrythmia diagnosis and follow up of pharmaceutical effects. A 24 h ECG measurement is conventionally called a "Holter" –measurement. Different number of measurement channels, from 1 to 12, are used in Holter-measurements with the placement of electrodes following approximately that of the 12 channel measurement setup. Applications of the long term ECG measurements include arrythmia diagnosis, monitoring of ST-segment, QT-time and the shape of the T-wave [13]. The application studied in detail in this work is monitoring and analysis of RR intervals, i.e. HRV analysis. When the detection of RR intervals is the main interest in the measurement, bandpass filters that emphasise the 10 Hz QRS complex can be used.

3.1.5 Sampling

The sampling frequency for ECG measurement should satisfy the Nyqvist sampling theorem, which means the sampling frequency should be at least twice as high as the highest frequency of the measured signal. Generally, in a clinical resting ECG, a sampling frequency of 500 Hz is used, while in high resolution ECG, 1000 Hz or higher values can be used [32]. For HRV analysis, the sampling frequency of ECG should be 500–1000 Hz [5] to resolve the very slow RR fluctuations also.

3.1.6 Electrode Material and Placement

Typically, disposable and adhesive silver-silver chloride (Ag-AgCl) surface electrodes are used on the thorax. In resting ECG, reusable electrodes are generally used around the wrists and the ankles, but in exercise and long term ECG, only disposable and adhesive electrodes are used. Ag-AgCl-electrodes are almost completely non-polarisable, meaning that no capacitative layer is formed on the electrode-skin-interface. This reduces artefact caused by electrode movement [42].

As in all biomedical signal measurement paradigms that utilize surface electrodes to measure a voltage produced by a subcutaneous tissue, to get best signal quality, the impedance on the electrode-skin-interface has to be equal on all electrodes. To achieve this most reliably, the impedance can be minimised by shaving the hair under the electrode, abrading the skin with e.g. sand paper and cleansing the skin with alcohol before attaching the pre-gelled electrode. The skin-electrode interface

should to be left to stabilise chemically for a short period of time before conducting the actual measurements [13, 42].

Electrical conduction over the skin-electrode interface can be further enhanced with added conductive paste or gel, if not included in the disposable electrode. Sweating and increased perfusion near the measuring site increase the electrical conductivity of the skin-electrode interface. Sweating or excess use of conductive gel may also cause short-circuiting of electrodes located very close to each other or loosening of electrodes from the skin [13].

3.1.7 Variability in ECG and Measurement Artefacts

There is always some variation in the ECG between subjects (interindividual variability), between measurement sessions for the same subject (intraindividual variability) and also between single heartbeats within the same measurement session (beat-to-beat variability) [35]. Measurement environment, instrumentation, and physiological factors affect the variability in the measured signal and can cause artefacts that interfere with the analysis of the signal and diagnosis.

Physiological Variability and Sources of Artefacts

There are numerous physiological factors that affect the ECG. The position and orientation of the heart vary interindividually and also intraindividually due to posture changes. Thus the direction of the currents from the heart vary also which affects the precision at which certain surface electrode positions can measure correct voltages [35].

The electrical activity of the skeletal muscles, the electromyogram (EMG), has most power in the frequency band of 5-400 Hz when measured on the skin [14]. Thus, it contains overlapping frequencies with the ECG signal, including the QRS complex, and can not be completely removed with frequency domain filtering. EMG activity originates from movement of the limbs, other muscular tension and shivering due to a cold environment. This is naturally inevitable in monitoring measurements and therefore a certain amount of low-pass filtering is needed, if e.g. only the frequency content of the QRS complex is of interest in the measurement.

Subject movement can also cause movement or complete disengagement of the electrodes and the electrode cables. Movement of the electrode cables can change the area of the current loops formed by the conductive skin and the cables. This phenomenon facilitates the contamination of the ECG signal by electromagnetic interference from external sources [35] (see more specifically in the next subsection).

Age, weight and ethnicity have been proven to have noticable effect on the measured ECG signal as well [35]. The effect of age is more pronounced during the age interval 10-18 years and the trends of change flatten after the age of 50 years. The age has an effect also on the occurrence rate of ventricular and supraventricular premature beats [35], where the conduction of the action potential from the SA node is for some reason blocked, and therefore the ventricles are activated by an action potential originating from either the AV node or from the Purkinje fibers, rather than by an SA node action potential.

Pregnancy increases heart rate and also cardiac output. Changes in body temperature, and therefore also eating and drinking affect the action potential conduction in the heart. Temperature changes have effects also on the autonomic nervous system control of the heart. Physical training increases cardiac muscle mass, increases the voltages of ECG, slows down the resting heart rate and increases the conduction times in the ventricles [35].

Technical Sources of Artefacts

Incorrect electrode placement of the precordial electrodes in the 12-channel ECG can lead to incorrect diagnosis and incomparability of the resulting signals to correctly measured signals [13, 35]. Training of measurement personnel is the most efficient way to deal with this type of artefacts.

Inadequate attachment and adhesion of the electrodes to the skin may cause disengagement of the electrodes and therefore abrupt baseline jumps in the ECG or complete loss of signal. Invalid choice of filters, sampling rate or electrode material, inadequate skin preparation or an amplifier input impedance of less than 5 MΩ may all constitute artefacts in the measured signal that can hamper analysis and diagnosis [35].

Electromagnetic interference from alternating current near the measurement site can produce a noticeable 50 or 60 Hz power line interference frequency component in the signal via capacitative coupling [13, 35]. This can be minimised by equalising the contact impedances of the electrode-skin-interfaces, using high input impedance amplifiers, shielding the electrode cables and by minimising the area of the current loops. The area can be reduced by simply using short cables between the electrode and the amplifier or by fixing the cables firmly to the skin. Longer cables can be wound around each other, creating current loops with reverse polarity, which nullify the effect of each other to some extent, i.e. using twisted pair cabling.

If the power line interference has contaminated the ECG signal, it may be removed via proper analog or digital filtering or advanced methods [19]. These post-processing methods can distort the signal or remove desirable frequency content, thus it is always preferable to optimise the measurement setting instead.

3.2 QRS Detection

The HRV time series can be formulated from an ECG measurement by detecting the occurrence of heart beats and calculating the time intervals between consecutive beats. To obtain the most direct information about the control of the ANS to the sinus node, heart beat occurrence times should be determined from the time points when action potential is generated in the SA node (see Chapter 2). The voltage induced between surface ECG electrodes by generation of the action potential in the SA node is very small and thus hard to distinguish from measurement noise.

The R wave is produced by depolarisation of the ventricles and it has the highest signal-to-noise ratio of all ECG waves in the surface ECG. This is because the ventricles have the highest cardiac muscle cell count of all parts of the heart and

because the cells depolarise virtually simultanously. Defining the heart beat occurrence time, and the HRV time series, based on the occurrences times of R waves thus gives heart beat detection the highest reliability.

There are several types of R wave peak detectors, or in a more broad sense, QRS detectors. Some detector algorithms are based simply on detecting the rising edge of the R wave through derivative operations, while more advanced algorithms use linear and nonlinear filters, different transformations and decision algorithms that adapt the function of the detector to changes in the ECG signal. Some QRS detectors utilise one ECG channel [18, 29] and some use several channels [7].

The accuracy of QRS detectors can be quantified by the metrics sensitivity s_{qrs} and positive predictivity p_{qrs} [18]:

$$s_{\text{qrs}} = \frac{\text{TP}}{\text{TP} + \text{FN}} \tag{3.1}$$

$$p_{\text{qrs}} = \frac{\text{TP}}{\text{TP} + \text{FP}}, \tag{3.2}$$

where TP = true positive, FP = false positive and FN = false negative. A false positive value means, that something else than an actual R wave was labeled as one. A false negative, on the other hand, is an actual manually verified R wave undetected by the algorithm. A detected R wave can be considered to be true positive, if it is in the range of $\pm$ 75 ms from the actual R wave [18].

A classical online QRS detector by Pan and Tompkins [29] is described here. The detector algorithm has been proven useful in presence of several kinds of ECG artefacts [30]. It contains the following four preprocessing steps. The input to each step is denoted with $x_i, i = 1, ..., N$ and the output with y_i.

1. 5–11 Hz digital bandbass filter to remove baseline trend and high frequency noise, and to amplify QRS complex frequencies.
2. Difference operator to emphasise fast changes in the signal:

$$y_i = \frac{1}{10}(2x_i + x_{i-1} - x_{i-3} - 2x_{i-4}), \tag{3.3}$$

   where N is the number of datapoints in the ECG signal. This filter approximates a linear derivative operator between frequencies 0–30 Hz [29].
3. Squaring operator:

$$y_i = x_i^2, \tag{3.4}$$

4. Moving average operator:

$$y_i = \frac{1}{W}\sum_{k=1}^{W} x_k \tag{3.5}$$

$$W = \frac{150\,\text{ms}}{f_s} \tag{3.6}$$

   where W is the window width of the moving average in number of datapoints and f_s is the ECG sampling frequency.

After preprocessing, the detector uses an adaptive threshold and a decision algorithm to categorise all positive deflections in the ECG to 1) R waves or 2) noise peaks. The decision algorithm uses average voltage of the R waves, average RR interval and physiological boundary values to adapt to changes in the ECG.

The variation in successive RR intervals can be very low in e.g. infants or subjects with low RSA, even in few milliseconds. Factors affecting in the accurate and precise detection of these changes are quality and sampling rate of the ECG, and an accurate QRS detector. The error due to a low sampling frequency has an especially large effect on spectral estimates of the HRV signal when the variation in RR intervals is small [25]. The recommended sampling rate for ECG meant for HRV analysis is 250 to 500 for healty adults, giving an precision requirement of $\pm$ 2 to $\pm$ 4 ms. For subjects with especially low-amplitude RR variation, sampling rate of 500 to 1000 Hz is recommended, giving $\pm$ 1 to $\pm$ 2 ms precision requirement [4, 33].

The HRV time series formulated from the R wave occurrence times (see Figure 3.3) can be visualised e.g. as a tachogram (see Figure 3.4a), where each heart beat interval is represented as a function of the interval number. The signal can also be represented as a time series (see Figure 3.4b), where the same heart beat intervals are represented as a function of the occurrence time of the end point of the interval. This time-series is naturally non-equispaced, if the RR interval is not constant during the whole measurement.

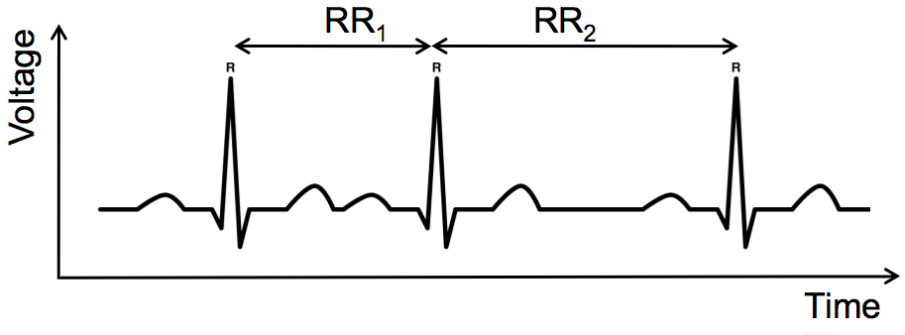

Figure 3.3: Construction of the HRV time series from RR intervals.

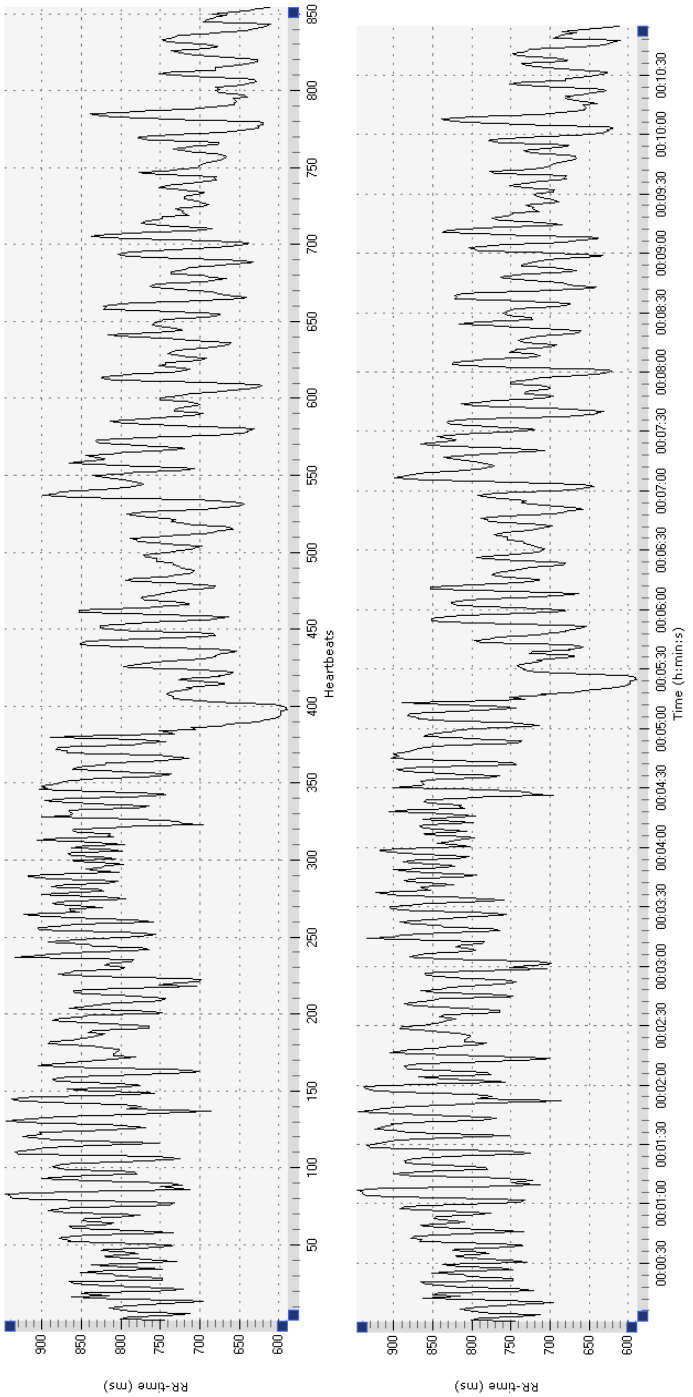

Figure 3.4: Visualisation of the measured RR intervals. a) Tachogram. b) Non-equispaced HRV time series.

Chapter 4

Analysis of Heart Rate Variability

There are several measures that can calculated from the HRV time series, including ones that express general parasympathetic or sympathetic activity. The calculated measures are used e.g. in prognosis of several diseases and in sports science. The analysis methods to gain these measures are generally divided into time domain, geometrical, frequency domain and nonlinear methods [38]. There are also different techniques to preprocess the HRV time series to render it suitable for certain time domain and spectrum estimation methods as well as techniques to detect and correct artefacts in the HRV time series. In this thesis, the attention is on some of the most popular time and frequency domain analysis methods.

4.1 Artefact Detection and Correction

Before the measured HRV time series is ready for trend removal or further analysis, possible measurement artefacts and strong deflections caused by physiological anomalies, including premature ventricular contractions, have to be accounted for. Because the goal of HRV analysis is to look at the ANS control over the heart rate, only normal heart beats initiated by SA action potentials can be included in the analysis as such. The artefacts cause significant bias especially in time and frequency domain estimates of HRV, while some geometrical and nonlinear methods are less vulnerable to artefacts [4].

The sections of a time series which contain these artefacts can be either excluded from the analysis altogether or corrected by some interpolation method. In some situations excluding data with artefacts could yield selection bias to the analysis results, rendering correction of the artefacts inevitable is these situations.

Most typical types of artefacts are missed or spurious QRS complexes between the actual ones. These are seen in the HRV time series as RR values about double or half value compared to the trend of the preceding and following data, and therefore these artefacts are somewhat simple to detect. Moving average or some other type of low-pass filter is one method to detect and to correct these outliers. Algorithms based on moving average usually reject RR values that differ more than a certain percentage from the average of a static number of past RR values [20]. The methods based on mean of past values can also have adaptive parameters, which allows

training of the algorithm to individuals [31].

Median filtering is an alternative to the low-pass approach in this problem. The upside of a median filter is the good ability to detect and correct impulse-like artefacts, while the downside is nonlinearity of the median operation, which renders the median filter ineligible for frequency domain examination.

4.2 Preprocessing

The HRV time series is a non-equispaced time series, if there is any variation in the RR intervals. Traditional spectral analysis methods, such as the Discrete Fourier Transform (DFT) and autoregressive (AR) modeling require the time series to be equispaced, stationary and zero-mean (see Section 4.5). The HRV time series can be morphed to an equispaced time series by e.g. linear or cubic spline interpolation and by sampling new, equispaced, data points from the interpolation functions.

Especially during long-term recordings and varying levels of physical activity, the HRV time series is non-stationary and it is, by definition, never zero-mean. Thus, trend removal methods must be applied before spectral analysis with the aforementioned methods can be carried out. For example, in measurements shorter than 5 minutes, VLF and slower frequencies do not contain reliable information, and can thus be discarded [38]. The effect of detrending on the estimates of LF frequencies is significant, especially when estimating the HRV spectrum with a low order autoregressive time series model (see Section 4.5) [37].

There are a number of trend removal methods available for HRV analysis. These include polynomial fits, low-pass filtering and advanced methods, such as smoothness priors. Smoothness priors is applied for the measurements conducted in this work. To understand the method, basics of least squares (LS) estimation have to be reviewed first.

Least Squares Estimation

Assume that we have measurements $x = (x_1, x_2, ..., x_N)^T \in \mathbb{R}^N$ taken at time instances $t_1, t_2, ..., t_N$, where $(\cdot)^T$ denotes the transpose operation. We can fit a model in this data, e.g. a linear observation model

$$x = H\theta + e, \tag{4.1}$$

where $H \in \mathbb{R}^{N \times p}$ is the observation matrix, $\theta = (\theta_1, \theta_2, ..., \theta_p)^T \in \mathbb{R}^p$ is a parameter vector describing the model and $e = (e_1, e_2, ..., e_N)^T \in \mathbb{R}^N$ is an observation error. If $p < N$, the system of equations $x = H\theta$ is overdetermined, and therefore no θ can satisfy the system of equations. Instead we have to find $\hat{\theta}$, an estimator for θ. The LS solution for $\hat{\theta}$ can be defined as the parameter vector θ that minimises the squared norm of the error [23]:

$$l(\theta) = ||e||^2 \tag{4.2}$$

$$= ||x - H\theta||^2, \tag{4.3}$$

where $||\cdot||$ is euclidian norm. It can be proven (see e.g. [16]) that the function (4.3) is minimised when the residual vector $x - H\theta$ is orthogonal to $R(H)$, a p dimensional subspace spanned by the columns of H. This orthogonality can be expressed as an inner product:

$$< x - H\hat{\theta}, H\theta >= 0, \quad \forall\theta, \tag{4.4}$$

where $\hat{\theta}$ is the best estimator for θ in LS sense, so that $H\hat{\theta} \in R(H)$. Now we can use this expression to solve the $\hat{\theta}$ that minimises the function (4.3):

$$(H\theta)^T(x - H\hat{\theta}) = 0, \quad \forall\theta \tag{4.5}$$

$$\theta^T H^T x - \theta^T H^T H\hat{\theta} = 0 \tag{4.6}$$

$$\theta^T(H^T x - H^T H\hat{\theta}) = 0 \tag{4.7}$$

$$< H^T x - H^T H\hat{\theta}, \theta >= 0. \tag{4.8}$$

Because this must be true for all θ,

$$H^T x - H^T H\hat{\theta} = 0 \tag{4.9}$$

$$H^T H\hat{\theta} = H^T x \tag{4.10}$$

$$\hat{\theta} = (H^T H)^{-1} H^T x, \tag{4.11}$$

where $(\cdot)^{-1}$ denotes the inverse matrix. The above solution exists, if $(H^T H)$ is an invertable matrix. To estimate values x in the time instances t according to the parameter estimates $\hat{\theta}$, the *prediction* of the model (4.1) can be used:

$$\hat{x} = H\hat{\theta}. \tag{4.12}$$

Smoothness Priors

Smoothness priors are a set of regularised variants of the least squares (LS) estimation method. The method presented here is an application to detrending the HRV time series, originally published in [37]. As the name of the method implies, it uses prior information the smoothness of the trend of the HRV time series. The measured RR intervals $x \in \mathbb{R}^N$ can be thought to be a sum of a smooth trend component $s \in \mathbb{R}^N$ and the underlying true HRV time series $u \in \mathbb{R}^N$:

$$x = s + u. \tag{4.13}$$

The trend s can be modeled with a linear additive observation model:

$$s = H\theta + e, \tag{4.14}$$

where $H \in \mathbb{R}^{Nxp}$ is the observation matrix, $\theta \in \mathbb{R}^p$ is the parameter vector of the LS regression, N is the number original datapoints and p is the number of parameters.

In smoothness priors, the minimised function is

$$l(\theta) = ||x - H\theta||^2 + \lambda^2 ||D_2 H\theta||^2, \tag{4.15}$$

where $\lambda \in \mathbb{R}$ is the smoothing parameter and D_2 is a difference operator, a discrete approximation of the second derivative:

$$D_2 = \begin{bmatrix} 1 & -2 & 1 & 0 & 0 & \dots & 0 \\ 0 & 1 & -2 & 1 & 0 & \dots & 0 \\ & & & \ddots & & & \\ 0 & \dots & 0 & 1 & -2 & 1 & 0 \\ 0 & \dots & 0 & 0 & 1 & -2 & 1 \end{bmatrix} \in \mathbb{R}^{N-2 \times N}. \tag{4.16}$$

The term $||x - H\theta||^2$ in the function (4.15) is the squared error norm seen in the LS estimation method and the term $\lambda^2 ||D_2 H\theta||^2$ is the regularisation term, which adjusts the effect of the squared norm of the second derivative of the prediction $H\theta$ on the minimised function. If $\lambda = 0$, no smoothing is applied, and the solution (parameter estimates $\hat{\theta}$ and prediction $H\hat{\theta}$) is the same as in the normal LS case. With higher values of λ, a smoother prediction for the trend is achieved.

Now we can write the function (4.15) in a form similar to (4.3), on which we can apply the LS solution (4.11):

$$\begin{aligned} l(\theta) &= (x - H\theta)^T (x - H\theta) + (\lambda D_2 H\theta)^T (\lambda D_2 H\theta) && (4.17) \\ &= \begin{bmatrix} (x - H\theta)^T (\lambda D_2 H\theta)^T \end{bmatrix} \begin{bmatrix} x - H\theta \\ \lambda D_2 H\theta \end{bmatrix} && (4.18) \\ &= \begin{bmatrix} x - H\theta \\ \lambda D_2 H\theta \end{bmatrix}^T \begin{bmatrix} x - H\theta \\ \lambda D_2 H\theta \end{bmatrix} && (4.19) \\ &= \left|\left| \begin{bmatrix} x - H\theta \\ \lambda D_2 H\theta \end{bmatrix} \right|\right|^2 && (4.20) \\ &= \left|\left| \begin{bmatrix} x \\ 0 \end{bmatrix} - \begin{bmatrix} H \\ \lambda D_2 H \end{bmatrix} \theta \right|\right|^2. && (4.21) \end{aligned}$$

This can be written as

$$\begin{cases} l(\theta) &= ||\tilde{x} - \tilde{H}\theta||^2 \\ \tilde{x} &= \begin{bmatrix} x \\ 0 \end{bmatrix} \\ \tilde{H} &= \begin{bmatrix} H \\ \lambda D_2 H \end{bmatrix} \end{cases} \tag{4.22}$$

and can therefore be solved with (4.11):

$$\hat{\theta} = (\tilde{H}^T \tilde{H})^{-1} \tilde{H}^T \tilde{x}. \tag{4.23}$$

This can be reduced to

$$\hat{\theta} = \left[\begin{bmatrix} H \\ \lambda D_2 H \end{bmatrix}^T \begin{bmatrix} H \\ \lambda D_2 H \end{bmatrix} \right]^{-1} \begin{bmatrix} H \\ \lambda D_2 H \end{bmatrix}^T \begin{bmatrix} x \\ 0 \end{bmatrix} \tag{4.24}$$

$$= \left[\begin{bmatrix} H^T & (\lambda D_2 H)^T \end{bmatrix} \begin{bmatrix} H \\ \lambda D_2 H \end{bmatrix} \right]^{-1} \begin{bmatrix} H^T & (\lambda D_2 H)^T \end{bmatrix} \begin{bmatrix} x \\ 0 \end{bmatrix} \tag{4.25}$$

$$= (H^T H + \lambda^2 H^T D_2^T D_2 H)^{-1} (H^T x). \tag{4.26}$$

When the only assumption of the trend s is smoothness, the observation matrix H can be chosen to be an identity matrix: $H = H^T = I \in \mathbb{R}^{N \times N}$. Therefore, we get

$$\hat{\theta} = (I + \lambda^2 D_2^T D_2)^{-1} x. \tag{4.27}$$

The prediction for the smooth trend component is thus

$$\hat{s} = H\hat{\theta} = \hat{\theta} = (I + \lambda^2 D_2^T D_2)^{-1} x \tag{4.28}$$

and the prediction for the underlying, nearly stationary, HRV time series from the function (4.13):

$$\hat{u} = x - \hat{s} = (I - (I + \lambda^2 D_2^T D_2)^{-1}) x. \tag{4.29}$$

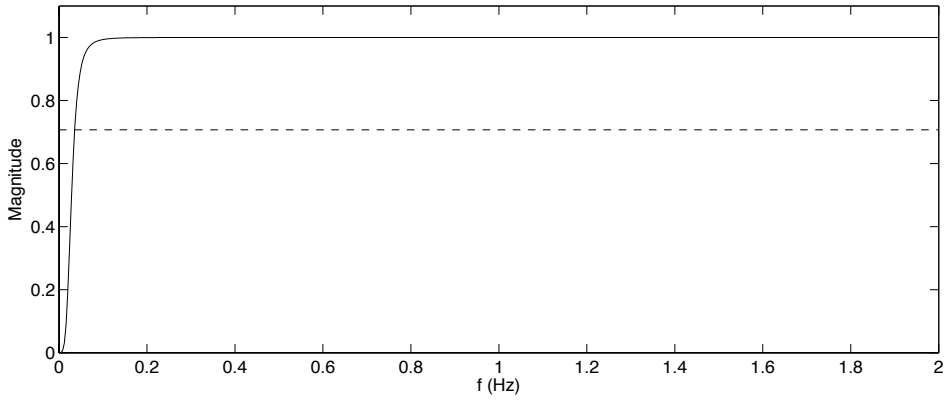

Figure 4.1: The frequency response of smoothness priors at the middle point. With a λ value of 500 and a sampling frequency of 4 Hz, the cutoff frequency (3 dB or $1/\sqrt{2} \approx 0.7$ attenuation) at this time point of the filter is 0.036 Hz.

The smoothness priors method can be thought of as a time-varying high-pass filter. For example, the Figure 4.1 shows the frequency response of the middle point of the smoothness priors filter. The cut-off frequency of the filter can be increased by decreasing the smoothing parameter λ, and vice versa. An advantage of the smoothness priors method is the ability to adjust the frequency response of the filter with just one parameter, compared to complicated multiparameter adjustment of a traditional high-pass filter, including order, ripple power and cut-off frequency adjustment. Another advantage of the smoothness priors method is that filtering of the data is strictest in the middle of the data and attenuated in the ends of data, which decreases distortion at the end points [37].

4.3 Time Domain Analysis Methods

The most straight forward HRV measures are time domain measures. The average RR value and the average HR value are

$$\overline{\mathrm{RR}} = \frac{1}{N}\sum_{j=1}^{N} \mathrm{RR}_j \tag{4.30}$$

$$\overline{\mathrm{HR}} = \frac{1}{N}\sum_{j=1}^{N} \frac{60}{\mathrm{RR}_j}. \tag{4.31}$$

A very popular measure describing overall variability in the HRV time series is the Standard Deviation of Normal-to-Normal beats (SDNN) [38], emphasising that only artefact free SA node originated data should be used in the calculation:

$$\mathrm{SDNN} = \sqrt{\frac{1}{N-1}\sum_{j=1}^{N}(\mathrm{RR}_j - \overline{\mathrm{RR}})^2}. \tag{4.32}$$

A measure of short term variability is the Root Mean Square of Successive Differences (RMSSD)

$$\mathrm{RMSSD} = \sqrt{\frac{1}{N-1}\sum_{j=1}^{N-1}(\mathrm{RR}_{j+1} - \mathrm{RR}_j)^2}. \tag{4.33}$$

When using time domain HRV measures, it is important to compare measurements of equal durations [38].

4.4 Geometric Methods

HRV Triangular index is defined as the ratio between the sum of the RR values and the maximum height of the histogram of the RR values, when the histogram bin width is 1/128 s [21]. The Triangular Interpolation of Normal-to-Normal interval histogram (TINN) is defined as the width of the base of a triangle fitted to the main peak in the histogram of the RR values. Both of these methods are insensitive to artefacts in the measured HRV time series, but require measurements with a duration of at least 20 minutes [38]. The HRV triangular index also correlates with the more error-prone SDNN measure [1], and therefore is a candidate for interchangeable use with the SDNN.

Another geometric analysis method is the Poincaré plot, which gives an estimate of the correlation between successive RR values. It is an ellipse fit to the scatter plot of RR_{j+1} as a function of RR_j. See [1, 36] for details.

4.5 Frequency Domain Analysis Methods

When measuring variability in a time series, intuitively the most natural tool for the task is spectrum analysis; either stationary or time-varying methods. The power

spectrum or power spectral density (PSD) contains information about how the power (i.e. variance) in the measured time series is distributed as a function of frequency. Frequency domain measures of HRV can subsequently be computed from the spectrum.

Spectrum estimation methods can be divided in two categories: parametric and non-parametric. The parametric methods include time series models such as the autoregressive (AR) model, the moving average (MA) model and the combination of these two: the ARMA model. Non-parametric methods, on the other hand, include e.g. methods based on the discrete Fourier transform (DFT) and methods based on wavelets. In this thesis, two spectrum estimation methods are presented and applied to HRV data: the stationary AR model and DFT based Welch's periodogram. The description of the methods presented here is based on [36], if not stated otherwise.

4.5.1 Stationarity

The spectrum estimation methods presented in this thesis require the input time series to be stochastic and stationary processes. A stochastic, i.e. random, process x_t, $t = 0, \ldots, N-1$ is a series of random variables. We can define expected value, or mean, $E\{x_t\}$ and autocorrelation $r_x(j,k)$ for this process:

$$E\{x_t\} = \int_{-\infty}^{\infty} xp(x_t)\mathrm{d}x \qquad \forall t = 0, \ldots, N-1 \tag{4.34}$$

$$r_x(j,k) = E\{x_j x_k\} \tag{4.35}$$

$$= \int_{-\infty}^{\infty}\int_{-\infty}^{\infty} x_j x_k p(x_j, x_k)\mathrm{d}x_j\mathrm{d}x_k \qquad j,k \in [0, \ldots, N-1], \tag{4.36}$$

where $p(\cdot)$ is the probability density function.

According to the most strict definition, a stochastic process is stationary only if no statistical properties of the process change as a function of time. A less strict, and more applicable, class of stationary processes is the class of wide-sense stationary processes, for which the mean $E\{x_t\}$ is constant $\forall t = 0, \ldots, N-1$ and the autocorrelation $r_x(j,k)$ depends only on the time lag $\tau = j - k$.

4.5.2 Autoregressive Spectrum Estimation

Stationary AR spectrum estimation is based on the assumption that the input time series x_t is a stationary AR process. This means that every data point x_t is determined by a white noise process e_t and the previous values of the time series $x_{t-1}, \ldots, x_{t-p}$, where $p \in \mathbb{N}$ is the order of the AR process. More precisely, an AR(p) process is

$$x_t = \sum_{j=1}^{p} a_j x_{t-j} + e_t, \tag{4.37}$$

where $(a_1, ..., a_p)^T = \theta$ are the coefficients of the AR(p) process [23]. An AR(p) process x_t can also be interpreted as the output of a linear time-invariant (LTI) system specified by θ, when the input signal to the system is white noise e_t. The phases of AR spectrum estimation are the following:

1. The model order p is first estimated somehow.
2. Then an AR(p) model is fit into the signal, the result of which are the AR(p) model coefficients θ.
3. Finally the coefficients θ are used to calculate the power spectrum estimate.

Model Coefficient Estimation

In an AR(p) model, the white noise term in the AR(p) process is replaced by a residual term ϵ

$$x_t = \sum_{j=1}^{p} a_j x_{t-j} + \epsilon_t, \tag{4.38}$$

which is then minimised in some sense to compute estimates for the model coefficients. Methods to do this include minimising the variance or the squared norm of the residual. The latter method is based on least squares, for which the system of equations (4.38) must be written in matrix form in the following way:

$$\begin{bmatrix} x_{p+1} \\ x_{p+2} \\ \vdots \\ x_N \end{bmatrix} = \begin{bmatrix} x_p & x_{p-1} & \dots & x_1 \\ x_{p+1} & x_p & \dots & x_2 \\ \vdots & & & \vdots \\ x_{N-2} & x_{N-3} & \dots & x_{N-p-1} \\ x_{N-1} & x_{N-2} & \dots & x_{N-p} \end{bmatrix} \begin{bmatrix} a_1 \\ a_2 \\ \vdots \\ a_p \end{bmatrix} + \begin{bmatrix} \epsilon_{p+1} \\ \epsilon_{p+2} \\ \vdots \\ \epsilon_N \end{bmatrix} \tag{4.39}$$

$$x = H\theta + \epsilon \tag{4.40}$$

$$\epsilon = x - H\theta. \tag{4.41}$$

The squared norm of the residual

$$||\epsilon||^2 = ||x - H\theta||^2 \tag{4.42}$$

is then minimised in LS sense (for comparison, see (4.3)) with the parameter estimate

$$\hat{\theta} = (H^T H)^{-1} H^T x. \tag{4.43}$$

Spectrum Estimation

To estimate the power spectrum of x_t using the estimated model coefficients $\hat{\theta}$ we define the AR(p) process as

$$x_t = -\sum_{j=1}^{p} a_j x_{t-j} + e_t. \tag{4.44}$$

By moving terms, by noting that $a_0 = 1$ and by implementing the z-transform on both sides of the equation we get

$$\sum_{j=0}^{p} a_j x_{t-j} = e_t \tag{4.45}$$

$$\sum_{j=0}^{p} a_j z^{-j} X(z) = E(z) \tag{4.46}$$

$$X(z) = \frac{E(z)}{\sum_{j=0}^{p} a_j z^{-j}}, \tag{4.47}$$

where $X(z)$ is the z-transform of x_t (system output) and $E(z)$ is the z-transform of e_t (system input). System function, also known as transfer function, $H(z)$ of an LTI system is defined as the ratio between the z-transform of the system output and z-transform of the system input. Therefore, for an AR system

$$H(z) = \frac{X(z)}{E(z)} = \frac{1}{\sum_{j=0}^{p} a_j z^{-j}} \tag{4.48}$$

$$X(z) = H(z)E(z). \tag{4.49}$$

The frequency response of an LTI system is $H(e^{i2\pi f/f_s})$, where i is the imaginary unit, f is frequency and f_s is the sampling frequency. In other words, the frequency response is the system function evaluated on the complex plane unit circle, where $z = e^{i2\pi f/f_s}$. The power spectrum of the AR process (i.e. the output from the AR system) is

$$P_{\mathrm{AR}}(f) = \left|X(e^{i2\pi f/f_s})\right|^2 \tag{4.50}$$

$$= \left|H(e^{i2\pi f/f_s})\right|^2 \left|E(e^{i2\pi f/f_s})\right|^2 \tag{4.51}$$

$$= \left|\frac{1}{\sum_{j=0}^{p} a_j e^{-i2\pi j f/f_s}}\right|^2 P_{e_t}(f), \tag{4.52}$$

where $P_{e_t}(f)$ is the power spectrum of white noise e_t, which is equal to σ_e^2/f_s i.e. constant by definition. Thus, we get for the power spectrum of the AR process

$$P_{\mathrm{AR}}(f) = \frac{\sigma_e^2/f_s}{\left|1 + \sum_{j=1}^{p} a_j e^{-i2\pi j f/f_s}\right|^2}. \tag{4.53}$$

Because the measured data is assumed to be the output from an AR system, we get the power spectrum of x_t by replacing the coefficients a_j with the coefficient estimates $\hat{a}_j$. The variance of white noise σ_e^2 is estimated with the variance of the residual σ_ϵ^2, also using the estimated coefficients $\hat{a}_j$

$$\hat{\sigma}_e^2 = \sigma_\epsilon^2 = \sigma_{x-H\hat{a}}^2. \tag{4.54}$$

Therefore, we get

$$P_{\mathrm{AR}}(f) = \frac{\sigma_\epsilon^2 / f_s}{\left|1 + \sum_{j=1}^{p} \hat{a}_j e^{-i2\pi j f / f_s}\right|^2}. \tag{4.55}$$

It is also possible to decompose the AR spectrum into separate components representing ULF, VLF, LF and HF bands, but this is not discussed in this work. For more information, see e.g. [23, 36].

Model Order Estimation

Usually in biosignal measurements, the exact characteristics of the physiological system generating the signal are unknown. Therefore, methods to estimate the optimal model order for e.g. spectrum analysis are required. Selection of the proper AR(p) model order to accurately model the underlying process owes to the principle of parsimony, also known as the Occam's Razor. It means that the simplest solution to a problem is usually the correct one. Thus, the lowest order model that sufficiently describes the signal at hand is the best choice [11].

We can quantize what is sufficient by e.g. examining the reduction in residual variance σ_ϵ^2 as the model order p is increased. Advanced model suitability criteria include the Final Prediction Error (FPE) [2], the Akaike Information Criterion (AIC), Corrected AIC for sequences shorter than 20 samples ($\mathrm{AIC_c}$), B-Information Criterion (BIC), the Minimum Description Length (MDL) [34] and the ϕ criterion (see reviews in [11, 36]):

$$\mathrm{FPE}(p) = \sigma_\epsilon^2 \frac{(N+p)}{(N-p)} \tag{4.56}$$

$$\mathrm{AIC}(p) = N \ln(\sigma_\epsilon^2) + 2p \tag{4.57}$$

$$\mathrm{AIC_c}(p) = N \ln(\sigma_\epsilon^2) + 2p + \frac{2(p+1)(p+2)}{N-p-2} \tag{4.58}$$

$$\mathrm{BIC}(p) = \mathrm{MDL}(p) = N \ln(\sigma_\epsilon^2) + p \ln(N) \tag{4.59}$$

$$\phi(p) = N \ln(\sigma_\epsilon^2) + p \ln(\ln(N)). \tag{4.60}$$

Iterating from AR(p) models with low order to ones with a higher order and calculating the residual variance for each model, so-called criterion curves as a function of model order can be calculated. With orders smaller than that of the actual process, $\sigma_\epsilon^2 >> \sigma_e^2$, which is called under-modeling. On the other hand, over-modeling, i.e. using models with higher order than the true one leads to only a minor decrease in σ_ϵ^2 [11].

The above mentioned criteria have similar properties to σ_ϵ^2. Thus, the best model order can be chosen near the order where the selected criterion function levels off or, in the optimal case, in the minimum of the criterion function. It must be noted though, that the above criteria have originally been developed for actual AR(p) processes and therefore they can be used only as guidelines when estimating the order biological systems, such as the autonomic nervous system, which regulates the

modulations in the measured HRV time series. It has been noted experimentally that AR models of order 8 to 20 describe the HRV times series sufficiently [38].

4.5.3 Welch's Periodogram

The discrete Fourier transform (DFT) of $x_t \in \mathbb{R}^N$, evaluated at frequencies $f_k = \frac{kf_s}{N}, k = 0, ..., N-1$ is

$$X_{\mathrm{DFT}}(f_k) = \sum_{j=0}^{N-1} x_j e^{-i2\pi jk/N} \tag{4.61}$$

which can be considered as the Fourier transform of an infinite periodic extension of x_t multiplied with a N point rectangular window. Fast Fourier Transforms (FFT) are algorithms that are used to calculate the DFT efficiently in terms of computational effort. The DFT is used in spectrum estimation methods such correlograms and periodograms. The fundamental periodogram power spectrum estimate for x_t is

$$P_{\mathrm{PG}}(f_k) = \frac{1}{Nf_s} \left| \sum_{j=0}^{N-1} x_j e^{-i2\pi jk/N} \right|^2 \tag{4.62}$$

which is the squared absolute value of DFT scaled with the term $\frac{1}{Nf_s}$. The rectangular window used in calculation renders an inherent spectral leakage property to the periodogram.

Averaging methods to reduce the variance and windowing methods to reduce the spectral leakage of the periodogram have been developed. These are generally called periodogram modifications. Welch's periodogram [45] is one of them, in which both averaging and windowing are utilised. Overlapping signal segments with a length of $D < N$ points are taken from x_t, yielding M number of segments $x_j^{(m)}$, where $j = 0, ..., D-1$ and $m = 1, ..., M$. Each segment is then multiplied by a window function w_j. After this, the average of the periodograms of these windowed segments is calculated:

$$P_{\mathrm{Welch}}(f_k) = \frac{1}{M} \sum_{m=1}^{M} \left(\frac{1}{Df_sU} \left| \sum_{j=0}^{D-1} w_j x_j^{(m)} e^{-i2\pi jk/D} \right|^2 \right), \tag{4.63}$$

where U is the energy of the window function w_j

$$U = \frac{1}{D} \sum_{j=0}^{D-1} w_j^2. \tag{4.64}$$

For example the Hanning window can be used for w_t. Both averaging and the use of overlapping segments reduce the variance of the estimate, but at the same time decrease the frequency resolution, when compared to the original periodogram (4.62).

4.5.4 HRV Measures

Typical frequency domain HRV measures are band powers and peak frequencies of each band calculated from the estimated power spectrum [38, 36]. Power of each spectral band (ULF, VLF, LF and HF) can be calculated

$$P_{[f_k,f_l]} = (f_1 - f_0) \sum_{j=k}^{l} P(f_j), \tag{4.65}$$

where f_k and f_l are the lower and higher border frequencies of the calculated spectral band, respectively.

The power of each spectral band can be expressed as an absolute value (in ms^2 or a similar unit) as above. Another way to express the band power is normalised to total power:

$$P_{[f_k,f_l]}(\%) = \frac{P_{[f_k,f_l]}}{P_{\mathrm{total}}} \times 100. \tag{4.66}$$

Yet another established way is to express band power in "normalised units" (n.u.), which is defined only for LF and HF bands:

$$P_{\mathrm{LF}}(\mathrm{n.u.}) = \frac{P_{\mathrm{LF}}}{P_{\mathrm{total}} - P_{\mathrm{VLF}} - P_{\mathrm{ULF}}} \tag{4.67}$$

$$P_{\mathrm{HF}}(\mathrm{n.u.}) = \frac{P_{\mathrm{HF}}}{P_{\mathrm{total}} - P_{\mathrm{VLF}} - P_{\mathrm{ULF}}}. \tag{4.68}$$

The ratio of absolute LF and HF powers, $P_{\mathrm{LF}}/P_{\mathrm{HF}}$, is also a popular measure of HRV, because is reflects the balance between sympathetic and parasympathetic activity [38].

To resolve if a measured HRV signal contains frequencies f, the length of the measurement has been recommended to be at least ten times the corresponding wavelength [38]. For example, to resolve LF and HF frequencies, the duration of the measurement has to be at least

$$t = \frac{10}{f_{\min}(\mathrm{LF})} = \frac{10}{0.04\,\mathrm{Hz}} \approx 4.2\,\mathrm{minutes}. \tag{4.69}$$

4.6 Nonlinear Analysis Methods

The more recently developed analysis methods of HRV are nonlinear in nature and able to describe complex systems, such as the autonomic nervous system, and are a promising direction of HRV analysis. These methods include calculation of approximate and sample entropy, detrended fluctuation analysis, correlation dimension analysis, calculation of largest Lyapunov exponent, calculation of fractal dimension, calculation of Hurst exponent and recurrence plot analysis. See [1] for a review.

Chapter 5

Measurement Systems

5.1 eMotion HRV

The eMotion HRV measurement system is a commercial measurement system developed by Mega Electronics Ltd, Kuopio, Finland. The system consists of a one channel RR interval sensor using ECG, a computer interface, data acquisition software and a docking station for recharging multiple sensors (see Figure 5.1).

Contribution of the author to product development of the eMotion HRV system was the design, implementation and testing of the data acquisition PC software, eMotion LAB. The product development of the system, including documentation and testing, was in compliance with the prevailing standards of the European Medical Device Directive (MDD) and the Food and Drug Administration (FDA) of the United States.

5.1.1 Sensor

The sensor measures one channel ECG with two electrodes. For measurement, two adhesive disposable electrodes are attached on the chest of the subject according to the placement seen in Figure 6.1 and the snap-on electrode connectors of the sensor are connected. The sensor weighs 16 g and is 35×35×15 mm in size, and therefore does not necessarily require any attachment method to the subject other than the adhesive electrodes.

The sensor measures the ECG signal with a sampling rate of 1000 Hz using a band-pass filter to maximise ECG power in the QRS complex frequencies. The amplitude resolution in ECG measurement is 1 μV / bit with a 12 bit analog-to-digital converter. The intervals between consecutive R waves are detected with an adaptive QRS detector, which uses measures based on the moving average of R wave amplitude and RR interval to categorise deflections in the measured ECG as R waves or noise peaks. The accepted RR intervals are stored in the memory of the sensor for later downloading. The sensor has 4 MB of flash memory and a Li-Ion battery with a capacity of 135 mAh, totalling to a measurement capacity of approximately eight consecutive days in room temperature and mild physical activity of the subject.

Figure 5.1: The eMotion HRV measurement system, containing the HRV sensor, the USB interface and the USB cable.

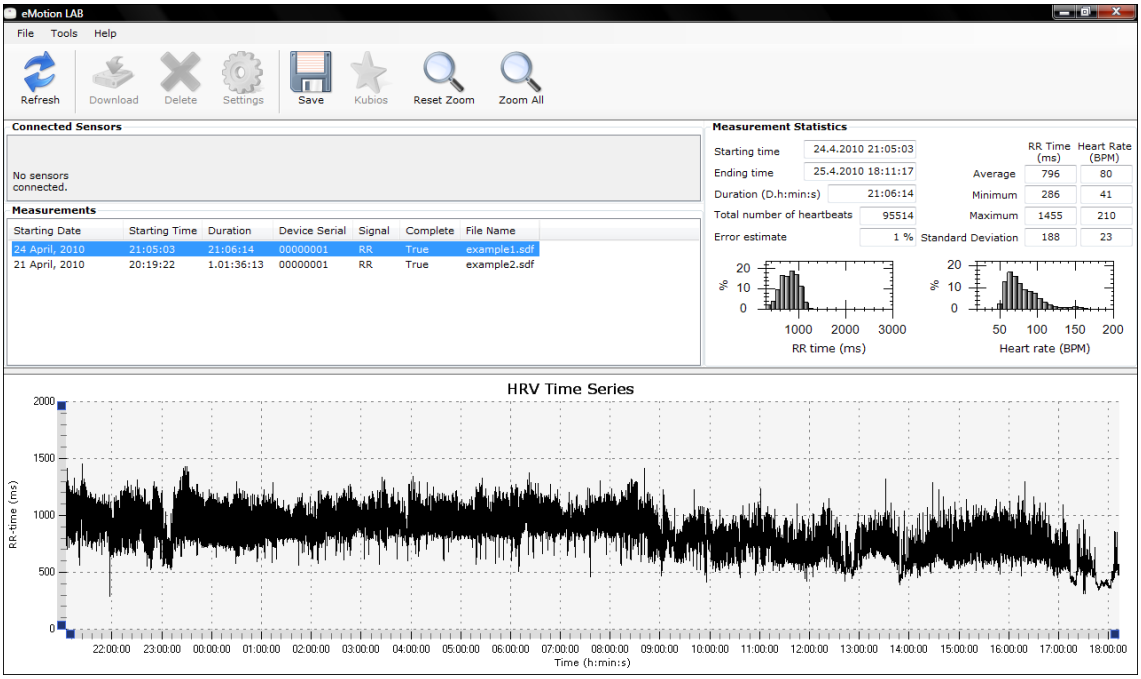

Figure 5.2: Screen shot of the eMotion LAB software.

5.1.2 Software Development Tools

The data acquisition software of the measurement system, eMotion LAB, was developed for the Windows platform, using the C# programming language version 3.0, the .NET Framework version 3.5, Service Pack 1, the Visual Studio 2008 integrated development environment (IDE) and the Windows Forms graphical application programming interface (API).

C# is a programming language developed by Microsoft and publicly released in 2000 as a part of the .NET software framework. The .NET framework is currently one of the main platforms used in Windows software design. C# has a similar syntax to C and C++ programming languages, but is fundamentally object oriented much in the same manner as Java. It has advanced features such as automatic memory management (garbage collection), generic data types and interoperability features with software and libraries outside the .NET framework. It has also attained a certification by the International Organization for Standardization [15].

Microsoft Visual Studio is an IDE for the Windows operating systems. It can be used to develop Windows applications in languages such as Visual Basic, C++ and C#. It contains integrated text editing, compiling, debugging and Windows Forms design features in one graphical user interface.

Windows Forms is one of the graphical APIs included in the Microsoft .NET framework and Visual Studio. Windows Forms applications are typically event driven, in which the user initiates the majority of activities performed by the application through a graphical user interface via e.g. clicking a button or entering a character string in a text box.

5.1.3 Software

The product development part of this thesis was to design and implement the data acquisition software eMotion LAB. It is meant for downloading measurement data from the eMotion HRV sensor, viewing and modifying sensor settings as well as reviewing and exporting the data to file (see Figure 5.2).

The sensor communicates with the computer with a device driver and an API. The sensor is shown as a serial COM port to the operating system, with which the eMotion LAB software communicates bidirectionally using the API. The API is written in C++ and therefore the interoperability features of the .NET framework were used to link the API to C# code.

A graphical user interface was designed and implemented for the software to allow the user to interact with the software with the use of events. The user interface contains a Windows Forms control for plotting and browsing the measurement files. The measurements can be viewed as tachograms or as non-equispaced HRV time series. The software shows also measurement metadata that is stored on the sensor and calculates simple statistical measures from the measurement, including the average, standard deviation, minimum and maximum of the RR and HR values as well as RR and HR histograms.

The measurement data with the metadata can be saved to an SDF file, which is formatted as an INI file containing ASCII data. The file format consists of a header

section for the metadata and of a data section for the RR values. The RR values are written in milliseconds, one value in each row. The SDF files can be opened in the eMotion LAB software later as well as in the Kubios HRV analysis software for further processing and analysis [28].

5.2 Cardiovit CS-200

The comparison system was a 12 channel exercise ECG system Cardiovit CS-200 with measurement software SDS-200 v. 2.45, manufactured by Schiller AG, Baar, Switzerland. The system is cleared by the MDD and the FDA for clinical stress ECG use. The system has 0.05 - 150 Hz measurement bandwidth, 500 Hz sampling frequency and 5 μV / bit amplitude resolution with a 12 bit analog-to-digital converter. The common mode rejection ratio of the ECG amplifier is higher than 100 dB and the input impedance 100 MΩ. The system also has defibrillation protection and pacemaker detection. The CS-200 system was connected to a bicycle ergometer Ergoselect 200 (Ergoline GmbH, Bitz, Germany) controlled programmatically from the CS-200 system.

Chapter 6

Materials and Methods

The performance of the eMotion HRV system in HRV measurement in different settings was validated by comparison to the commercial system Cardiovit CS-200. The measurements comprised of two laboratory experiments: an orthostatic experiment and an exercise experiment, and a 24 hour normal daily activity experiment. In the orthostatic and exercise measurements both measurement systems were used simultaneously, while in the daily activity measurement only the eMotion HRV system was used. A QRS detection algorithm was developed and implemented for ECG data obtained from the CS-200 system.

The HRV time series obtained from the orthostatic and exercise experiments were compared using histogram and Bland-Altman analysis. In addition, selected HRV parameters were calculated from the orthostatic experiment data and compared between the systems. Data from the daily activity experiment was analysed using activity diaries and an artefact detection algorithm developed in this work. All the detection and analysis algorithms as well as data visualisation were implemented in the Matlab environment (MathWorks Inc, MA, USA), totalling to 2803 lines of code in Matlab script and functions.

6.1 Subjects

The subjects of the measurements were healthy young adults in normal physical condition, one female and four males. The age (mean $\pm$ σ) of the subjects was (25.8 $\pm$ 2.2) years, the weight (71.6 $\pm$ 6.5) kg, the height (174.5 $\pm$ 6.8) cm and the body-mass index (23.5 $\pm$ 1.3) $\frac{\mathrm{kg}}{\mathrm{m}^2}$.

6.2 Measurements

6.2.1 Electrode Placement

The ECG electrode positions used in the orthostatic and exercise experiments can be seen in the Figure 6.1. Twelve ECG channels were measured with the CS-200 system using the Mason-Likar exercise ECG electrode positions (Figure 3.2). HRV time series derived from the channel II was used as the comparison for the eMotion

HRV system due to the parallel electrode positions. Rest of the channels were used to check for occurrence of ectopic beats.

For both the orthostatic and exercise experiments, disposable and adhesive electrodes Blue Sensor M (Ambu A/S, Ballerup, Denmark) were used. The skin under the electrodes was shaved when it was necessary and cleansed with alcohol before electrode attachment.

The electrodes and the cables were firmly attached to the patient with tape and with a wide elastic belt to reduce cable and electrode movement artefacts. The electrode cables were also wound around each other to minimise the area of the cable loops and therefore to diminish the 50 Hz powerline artefact.

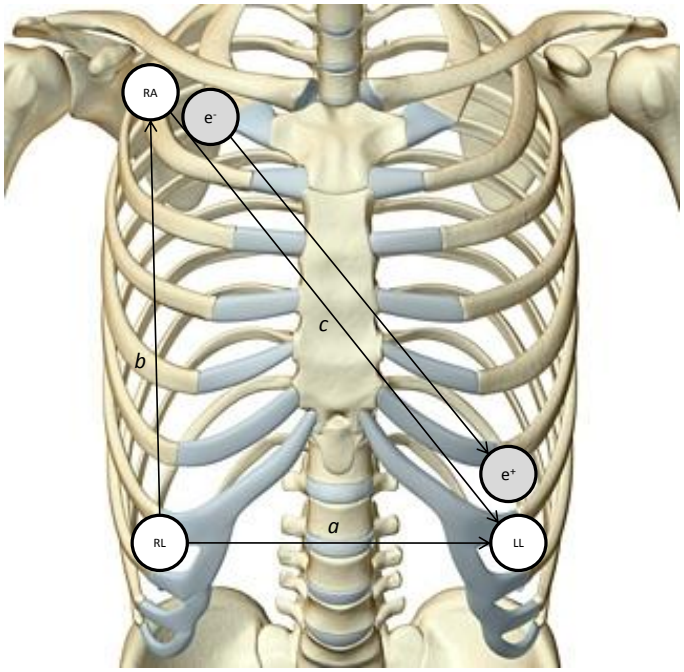

Figure 6.1: The locations of the measurement electrodes and the polarity of the measurement channels for HRV measurements during the orthostatic experiment and the exercise experiment. e^+ stands for the positive electrode of the eMotion HRV system and e^- the negative electrode. The signal of the channel II (vector c) can be derived from the two measurements (vectors a and b): $a - b = (\mathrm{LL} - \mathrm{RL}) - (\mathrm{RA} - \mathrm{RL}) = \mathrm{LL} - \mathrm{RA} = c = \mathrm{II}$.

6.2.2 Orthostatic Experiment

The first part of the measurements was the orthostatic experiment [43], where the subject lay relaxed in the supine position for five minutes, stood up and remained standing for another five minutes, while the HRV time series was recorded with both systems. The subject lay relaxed for a period of five minutes before the beginning of the measurement.

6.2.3 Exercise Experiment

In the exercise experiment the subjects cycled on the Ergoselect 200 ergometer for 13 minutes. The load of the ergometer was light in the beginning and in the end of the experiment, with a higher load level in the middle (Table 6.1).

Table 6.1: Measurement protocol

Phase	Load (W)	Duration (min:s)
Warm up	100	5:00
Exercise	175	3:00
Cool down	100	5:00

6.2.4 Long-term Daily Activity Experiment

In the long-term daily activity experiment, the HRV of the subjects was monitored for a 24 hour period with the eMotion HRV measurement system. The subjects were instructed to fill a diary table of their activities during the measurement period to track possible causes of artefacts in the measured time series. The diary was advised to be filled with 30 minute precision.

In the daily activity experiment, disposable surface electrodes Blue Sensor R (Ambu A/S, Ballerup, Denmark) were used. The recommended maximum time to wear the electrodes is 24 hours. The skin under the electrodes was shaved when it was necessary and cleansed with alcohol before electrode attachment. The electrode cables were attached to the body with tape to diminish electrode and cable movement artefacts.

6.3 Analysis

6.3.1 Generation of the Reference HRV Time Series

The HRV time series from CS-200 ECG data was generated using a QRS detector based on the Pan-Tompkins algorithm [29], as described in the Subsection 3.2. ECG channel II was used as algorithm input and the ECG signal was upsampled to a sampling frequency of 2 kHz before QRS detection using cubic spline interpolation to increase the precision of the reference RR values. The occurrence times of the detected R waves were verified visually (see Figure 6.2). The two HRV time series were temporally synchronised after measurements by matching the shapes of the time series and removing the non-overlapping data.

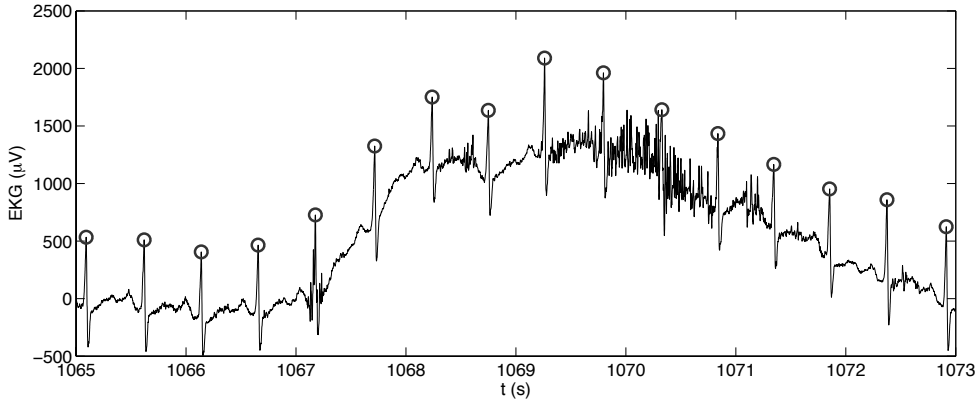

Figure 6.2: Example of performance of the QRS detector developed on the ECG signal measured with CS-200 system containing baseline wander and EMG artefact. The detected R wave peaks are shown with (o).

6.3.2 QRS Detection Accuracy Evaluation

The accuracy of the eMotion HRV QRS detector during the orthostatic experiment and during the exercise experiment was assessed using sensitivity and positive predictivity measures, see equations (3.1, 3.2). The R wave occurrence times measured by the eMotion HRV system were verified visually using the CS-200 ECG measurement as reference.

6.3.3 QRS Detection Precision Evaluation

The RR intervals calculated from the correctly detected R waves in the orthostatic and the exercise experiments were compared between the systems. The precision of eMotion HRV QRS detection was assessed by analysing the difference between the systems with a histogram of differences and a Bland-Altman plot [3]. The Bland-Altman plot is a scatter plot of the differences between the compared sequences as a function of the average of the sequences. Limits of agreement (LoA) (mean $\pm$ 2σ) were also calculated and plotted on the scatter plot to quantise the differences. The Gaussian shape of the distribution of differences was confirmed with the histogram.

6.3.4 Comparison of HRV Measures

The data from the orthostatic experiment was used to calculate a set of selected time and frequency domain HRV measures both for the supine and the standing measurement phases. These measures were then compared between the systems. Stationary signal segments with a duration of five minutes were used for HRV measure calculations. The time domain measures were $\overline{\mathrm{RR}}$, $\overline{\mathrm{HR}}$, SDNN and RMSSD.

$\overline{\mathrm{RR}}$ and $\overline{\mathrm{HR}}$ were calculated directly from the measured HRV time series. For calculation of SDNN and RMSSD, the time series were 1) cubic spline interpolated with 4 Hz sampling frequency (see Figure 6.3), 2) detrended with the smoothness

priors method, and 3) cubic spline interpolated at the original time points of the R waves (see Figure 6.4). In the resulting time series, the differences between successive RR intervals was the same as in the original measured HRV time series, but the trend had been removed, which is the requirement for SDNN and RMSSD calculation.

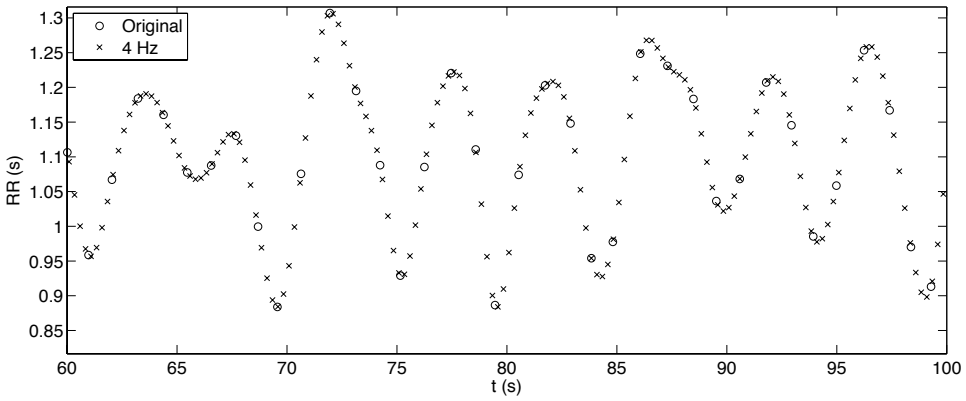

Figure 6.3: Example segment demonstrating the cubic spline interpolation of a measured HRV time series. The original non-equispaced values are shown with (o) and the spline functions sampled with a 4 Hz sampling frequency are shown with (×).

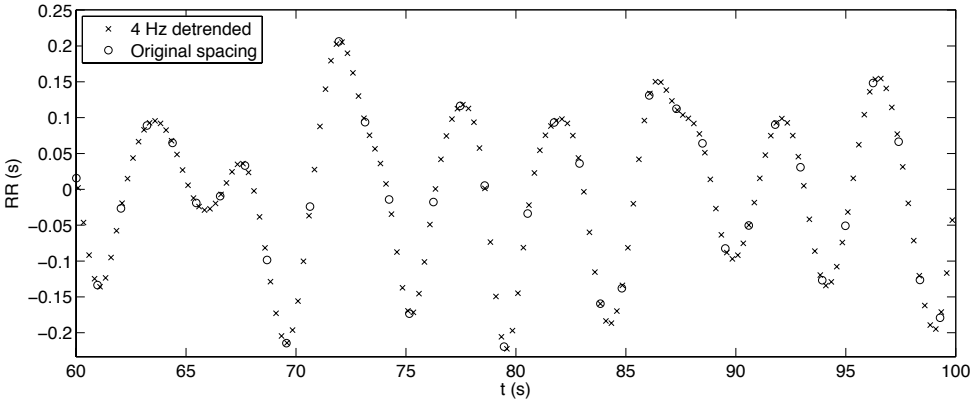

Figure 6.4: Cubic spline interpolation of the detrended HRV time series. The detrended equispaced data is shown with (×) and the RR values evaluated at original locations are shown with (o).

The calculated frequency domain measures were P_{LF}, P_{HF}, $P_{\mathrm{LF}}/P_{\mathrm{HF}}$ and P_{total}. The frequency domain estimates were calculated from both Welch's periodogram and AR(16) spectrum estimates. For spectrum estimation, the HRV time series were first cubic spline interpolated with 4 Hz sampling frequency, and then detrended with the smoothness priors method, thus producing a zero-mean, stationary and equispaced time series, all requirements of the spectrum estimation methods used. For Welch's periodogram, the Hanning window, 256 s window width and 50 % segment overlap were used. The AR(16) model coefficients were estimated using the LS method, the spectrum estimate was evaluated with 4096 points and the optimality of the model order was assessed with FPE, AIC and MDL criteria.

6.3.5 Analysis of Daily Activity Data

Artefacts in the HRV time series during the daily activity measurement were detected with an artefact detection algorithm consisting of a three-point median filter and comparison between the measured time series and the median filtered time series. The algorithm labeled RR intervals as artefacts, if they were 1) higher than 1.5 times the corresponding median filtered value, 2) lower than 0.5 times the corresponding median filtered value or 3) higher than 10 s. The $\pm$ 50 % threshold value was selected empirically to best detect artefacts for the measurements gained from all of the five test subjects.

According to the labels, an artefact ratio $\mathrm{N}_{\mathrm{artefacts}}/\mathrm{N}_{\mathrm{all}}$ was calculated for each measurement. The activities reported in the activity diaries were then correlated qualitatively with the occurrence of artefacts in the measurements.

Chapter 7

Results and Discussion

In this chapter, the measured data and results of analysis from the orthostatic, exercise and daily activity experiments will be reviewed. Inferences about the accuracy and precision of the QRS detection capability of the eMotion HRV system and its effects on HRV measures calculated from the data will be made. In addition, the applicability of the eMotion HRV system to long-term ambulatory measurements will be made based upon the results of the analysis.

7.1 QRS Detection Accuracy Evaluation

Data from the orthostatic and exercise experiments was used to assess the accuracy of the eMotion HRV QRS detector using sensitivity and positive predictivity measures and manual verification. Regarding the ECG signal measured from the study population by the CS-200 system as the reference, all R waves were identified correctly by the eMotion HRV system in the orthostatic experiment, and one R wave was misdetected during the exercise experiment. Thus, sensitivity and positive predictivity for the QRS detector of eMotion HRV in this study population were

$$s_{\mathrm{qrs}} = 99.989\,\% \tag{7.1}$$

$$p_{\mathrm{qrs}} = 99.989\,\%. \tag{7.2}$$

These are very high figures, and show that the data procuded by the eMotion HRV system is accurate for a normal, healthy population.

7.2 QRS Detection Precision Evaluation

The HRV time series of one subject measured with both systems in the orthostatic experiment can be seen in the Figure 7.1. There is a five minute wide-sense stationary segment in the beginning of both time series, followed by a rapid decrease in the RR intervals compensating the redistribution of blood volume due to standing up. The RR intervals settle by average at a lower level in the standing phase than in the supine phase and another five minute wide-sense stationary segment can be seen in the end of the measurement. The differences between the time series are in the order of milliseconds, and can not thus be easily distinguished from the figure in question.

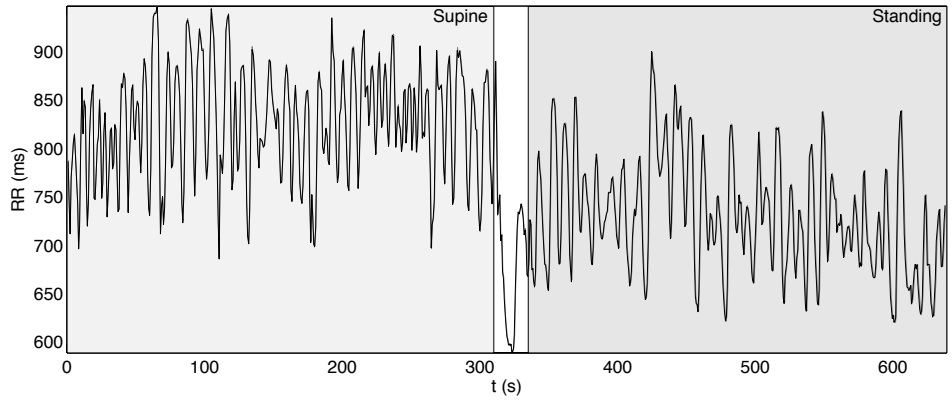

Figure 7.1: The HRV time series of one subject measured with both systems in the orthostatic experiment. eMotion HRV data is shown with grey and CS-200 data is shown with black.

The HRV time series of one subject from the exercise experiment can be seen in the Figure 7.2. The strong fluctuations in the RR intervals due to climbing on the ergometer can be seen in the beginning of the time series, followed by a decreasing trend in the mean and variance of the RR intervals during the five minute period of light ergometer load. The mean and variance of RR values decrease significantly after the increase in the ergometer load from 100 W to 175 W, only to increase again during the following period of light load and the relaxation period in the end of the experiment. Again, the point-to-point differences are difficult to distingish from the figure at hand.

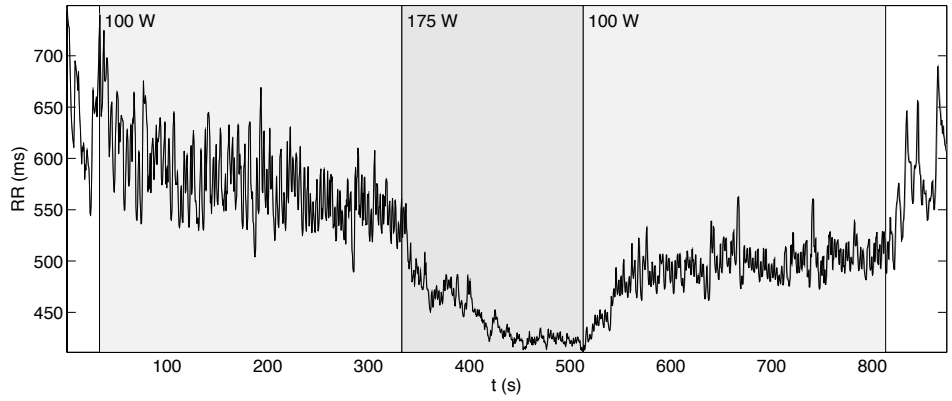

Figure 7.2: The HRV time series of one subject measured with both systems in the exercise experiment. eMotion HRV data is shown with grey and CS-200 data is shown with black.

The differences in individual RR values

$$\Delta RR = RR_{\text{eMotion HRV}} - RR_{\text{CS}-200} \tag{7.3}$$

can be seen more easily with the histograms of differences and the Bland-Altman plots. Compound data from all five subjects in the orthostatic experiment is shown in the Figure 7.3, and all exercise experiment data is shown in the Figure 7.4. The differences between RR intervals in the Bland-Altman plot are quantized in clusters with a spacing of 0.5 ms due to finite precision of 2 kHz and 1 kHz of the ECG signals used in HRV time series generation. The LoA ($\overline{\Delta RR} \pm 2\sigma_{\Delta RR}$) of the Bland-Altman plots, for each subject individually and for compound data, are listed in the Table 7.1. For all future measurements, the difference in RR intervals between the systems lies between the LoA with a probability of approximately 95 %.

Table 7.1: Mean $\overline{\Delta RR}$ and double standard deviation $2\sigma_{\Delta RR}$ of the differences between systems in Bland-Altman analysis.

Orthostatic experiment			Exercise experiment		
Subject(s)	$\overline{\Delta RR}$ (ms)	$2\sigma_{\Delta RR}$ (ms)	Subject(s)	$\overline{\Delta RR}$ (ms)	$2\sigma_{\Delta RR}$ (ms)
1	0.643	1.510	1	0.385	2.174
2	0.635	1.511	2	0.403	2.218
3	0.649	1.640	3	0.298	2.007
4	0.570	1.424	4	0.231	1.940
5	0.909	1.629	5	0.446	2.241
All	0.670	1.557	All	0.343	2.109

During the analysis, a temporal lag between the internal clocks of the measurement systems was detected. The cumulative temporal lag was approximately 421 ms during a 500 s measurement, which is equal to 0.8 % lag. This lag caused a small bias in the RR value differences seen in the Table 7.1. This lag is not present when two eMotion HRV sensors are compared, and thus the bias was corrected for accurate analysis of the QRS detection precision of eMotion HRV. This was achieved by scaling the measurements from different systems to equal duration. After the scaling operation, the Bland-Altman analysis was conducted for the absolute value of differences between individual RR values ($\overline{\Delta RR}$), and the results listed in the Table 7.2 were obtained.

The differences between systems can be explained partly by differences in the QRS detectors. Especially, the eMotion HRV system detects peaks of the R waves from band-pass filtered ECG with slightly rounded peaks, while the QRS detector developed in this work used the raw ECG with a bandwidth of 0.05 - 150 Hz in R wave peak detection. Other possible factors increasing the variance of the RR value differences could be the fluctuations in the distances between measurement electrodes and the heart as well as changes in conduction velocities due to movement of the thorax. The larger variance of differences during the exercise experiment strengthens this hypothesis.

Table 7.2: Mean $\overline{|\Delta RR|}$ and double standard deviation $2\sigma_{|\Delta RR|}$ of the absolute value of differences between the systems in Bland-Altman analysis for measurements scaled to equal duration.

Orthostatic experiment			Exercise experiment		
Subject(s)	$\overline{\lvert\Delta RR\rvert}$ (ms)	$2\sigma_{\lvert\Delta RR\rvert}$ (ms)	Subject(s)	$\overline{\lvert\Delta RR\rvert}$ (ms)	$2\sigma_{\lvert\Delta RR\rvert}$ (ms)
1	0.600	0.895	1	0.858	1.330
2	0.582	0.944	2	0.893	1.308
3	0.631	1.035	3	0.806	1.186
4	0.545	0.849	4	0.765	1.187
5	0.592	1.089	5	0.824	1.500
All	0.591	0.962	All	0.820	1.308

To summarise, the precision of QRS detection of the eMotion HRV system was in this population ± 0.962 ms during rest and ± 1.308 ms during exercise, when the absolute RR value differences of duration scaled measurements were assessed. These values fulfill even the requirements of QRS detection precision for individuals with low-amplitude RR variation of ± 1 to ± 2 ms for HRV analysis [4], and thus validates the measurement precision of the eMotion HRV system for HRV analysis. To put the values into perspective, the precision is superior compared to the LoA of -12.4 to 11.5 ms and -15.1 to 14.3 ms determined in a validation study of two ambulatory HRV measurement devices, which use chest strap electrodes [44].

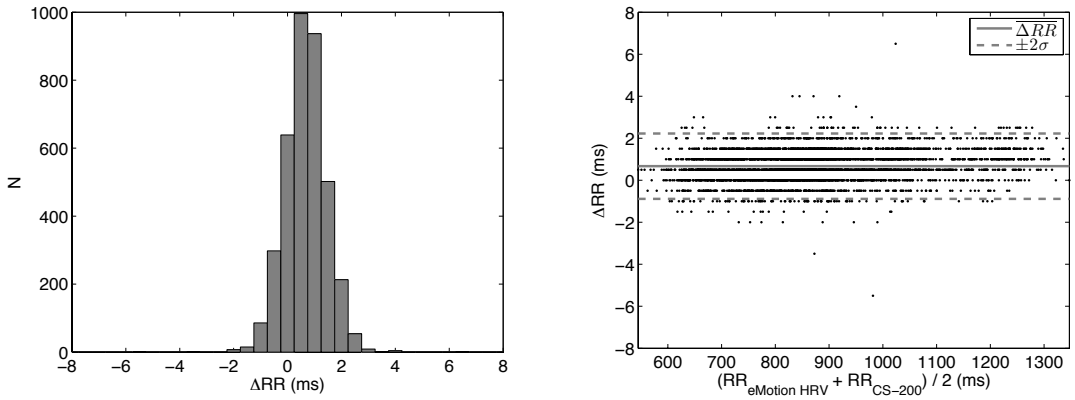

Figure 7.3: Histogram of differences and Bland-Altman plot of the orthostatic experiment.

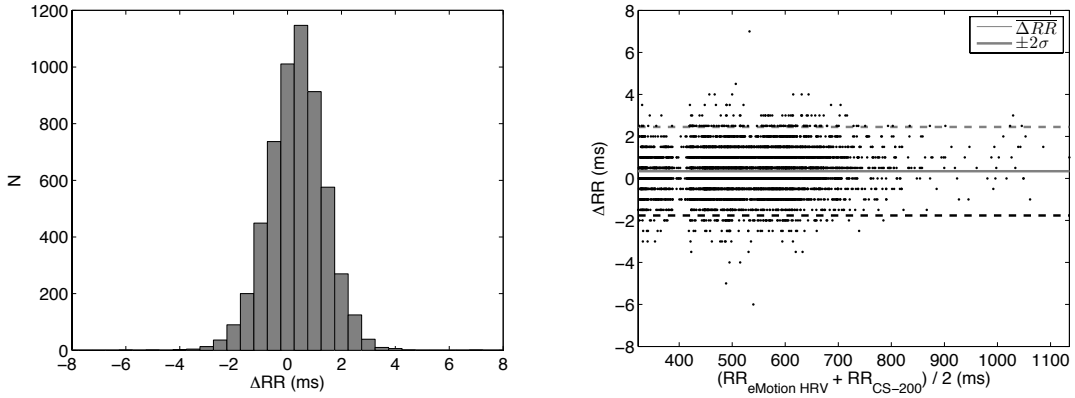

Figure 7.4: Histogram of differences and Bland-Altman plot of the exercise experiment.

7.3 Comparison of HRV Measures

Two HRV segments with a duration of five minutes from the orthostatic experiment were used for estimation of HRV measures for each subject. The original measurement, the estimated trends and the interpolated and detrended segments used for frequency domain HRV measure estimation are shown in the Figure 7.5. The the absolute differences in HRV measures θ between systems (eMotionHRV − CS200) and relative differences in the HRV measures between systems ((eMotionHRV − CS200)/CS200) are listed in the Tables 7.3 and 7.4.

For spectrum estimation, the criterion curves for estimation of the optimal AR model order were plotted and are shown in the Figure 7.6. Based on the minima of the curves, 16 was chosen as the order for all AR spectrum estimation models.

For detailed assessment of the differences between the measurements on frequency domain HRV measures, the spectrum estimates and the difference between the spectrum estimates were plotted in the Figures 7.7 and 7.8. The differences in the spectrum estimates are not visible when plotted upon the other, but the difference plot reveals the subtle deviations.

The magnitude of the effect of the spectrum estimate differences can be seen in the Tables 7.3 and 7.4. At most, the relative difference between systems of any of the calculated HRV measures was 1.61 % (AR(16) P_{LF}), while the smallest difference was 0.06 % ($\overline{\mathrm{RR}}$).

The effect of the time lag between the system clocks on the HRV measures was assessed also. The HRV measures were calculated from data scaled to equal duration and the population averages of differences between systems was calculated for each each HRV measure. The population average differences for both original unscaled data and scaled data are shown in the Table 7.5. The absolute value of all population average differences were below 1 % for the unscaled data and below 0.72 % for the scaled data. The differences are very small and demonstrate the validity of the eMotion HRV system for HRV measurement.

Table 7.3: Calculated HRV measures with the absolute and relative differences for one subject for the supine segment.

HRV Measure	CS-200	eMotion HRV	Absolute Difference	Relative Difference (%)
$\overline{\text{RR}}$ (ms)	1034.597	1035.325	0.728	0.07
$\overline{\text{HR}}$ (BPM)	57.994	57.953	-0.041	-0.07
SDNN (ms)	105.363	105.519	0.156	0.15
RMSSD (ms)	127.819	128.037	0.218	0.17
Welch P_{LF} (ms^2)	1467.447	1476.725	9.278	0.63
Welch P_{HF} (ms^2)	8801.040	8829.558	28.518	0.32
Welch $P_{\text{LF}}/P_{\text{HF}}$	0.167	0.167	0.001	0.31
Welch P_{total} (ms^2)	10519.177	10559.000	39.823	0.38
AR(16) P_{LF} (ms^2)	1466.875	1469.835	2.959	0.20
AR(16) P_{HF} (ms^2)	8971.349	9013.205	41.855	0.47
AR(16) $P_{\text{LF}}/P_{\text{HF}}$	0.164	0.163	-0.0004	-0.26
AR(16) P_{total} (ms^2)	10719.696	10766.235	46.539	0.30

Table 7.4: Calculated HRV measures with the absolute and relative differences for one subject for the standing segment.

HRV Measure	CS-200	eMotion HRV	Absolute Difference	Relative Difference (%)
$\overline{\text{RR}}$ (ms)	735.959	736.430	0.471	0.06
$\overline{\text{HR}}$ (BPM)	81.526	81.474	-0.052	-0.06
SDNN (ms)	59.845	59.906	0.060	0.10
RMSSD (ms)	47.008	47.029	0.021	0.04
Welch P_{LF} (ms^2)	1705.877	1710.476	4.599	0.27
Welch P_{HF} (ms^2)	1689.118	1691.423	2.305	0.14
Welch $P_{\text{LF}}/P_{\text{HF}}$	1.010	1.011	0.001	0.13
Welch P_{total} (ms^2)	3535.677	3543.454	7.777	0.22
AR(16) P_{LF} (ms^2)	1947.793	1970.353	22.560	1.61
AR(16) P_{HF} (ms^2)	1409.614	1421.087	11.473	0.81
AR(16) $P_{\text{LF}}/P_{\text{HF}}$	1.382	1.387	0.005	0.34
AR(16) P_{total} (ms^2)	3680.180	3715.356	35.177	0.96

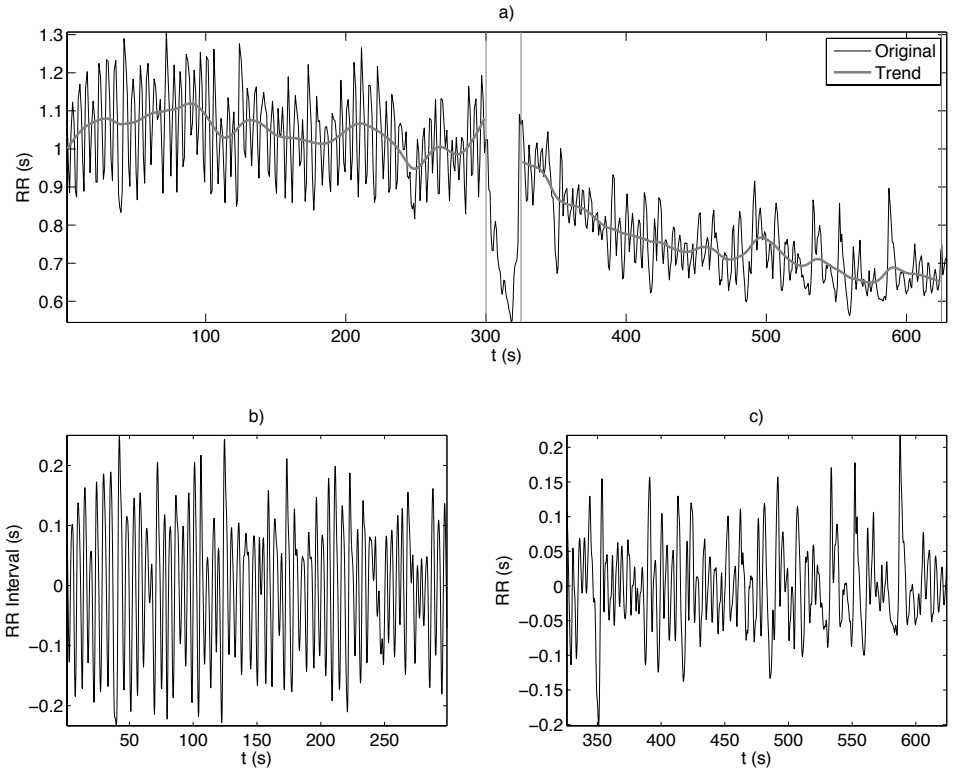

Figure 7.5: a) The original measurement, segments chosen for HRV measure estimation and the estimated trends. b) The interpolated and detrended supine segment. c) The interpolated and detrended standing segment.

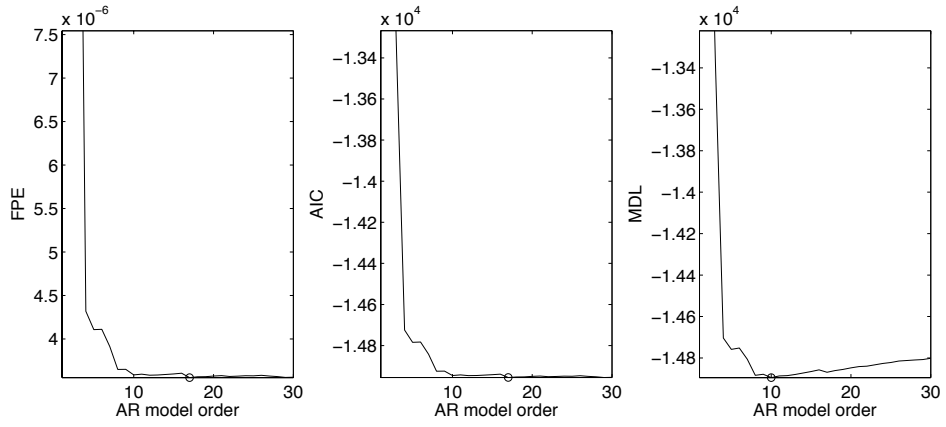

Figure 7.6: Estimation of the optimal AR model order for spectrum estimation for the supine phase of one subject using the FPE, AIC and MDL criteria. Model orders at the local minima (o) of the three criterion functions in the interval [1, 30] were 17, 17 and 10, respectively.

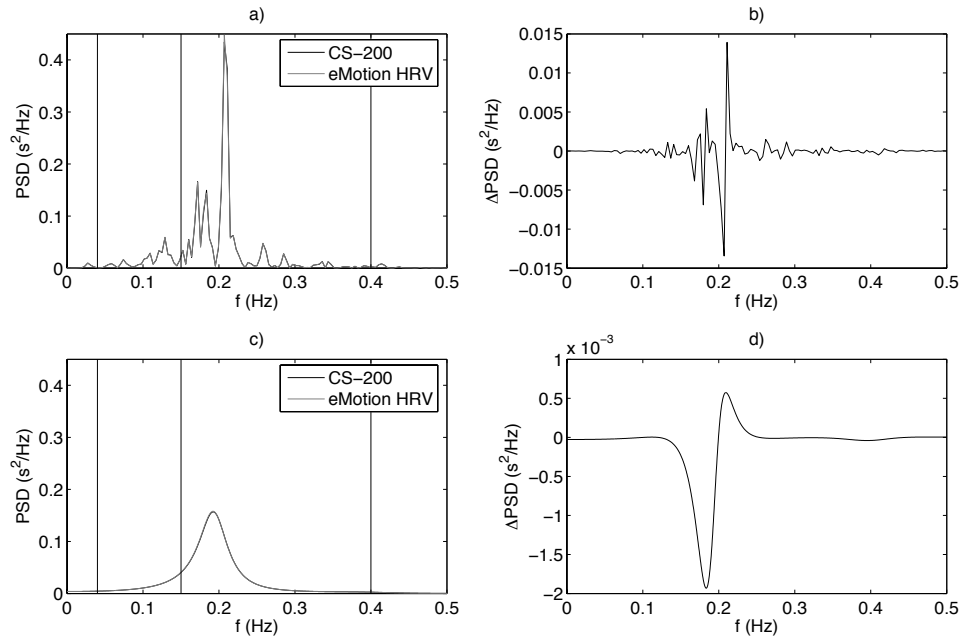

Figure 7.7: The spectrum estimates and differences of spectrum estimates for the supine phase of the orthostatic experiment. a) Welch's periodogram, spectrum estimates from both systems. b) Welch's periodogram, difference between systems. c) AR(16), spectrum estimates from both systems. d) AR(16), difference between systems.

Table 7.5: Population averages of the relative differences between systems for each HRV measure. The averages are calculated for both original and temporally scaled measurements.

	Unscaled data		Scaled data	
HRV Measure	Supine (%)	Standing (%)	Supine (%)	Standing (%)
$\overline{\text{RR}}$	0.079	0.075	0.002	-0.001
$\overline{\text{HR}}$	-0.079	-0.075	-0.002	0.001
SDNN	0.211	0.105	0.140	0.044
RMSSD	0.275	0.217	0.204	0.146
Welch P_{LF}	0.342	0.143	0.165	0.004
Welch P_{HF}	0.093	0.431	0.031	0.515
Welch $P_{\text{LF}}/P_{\text{HF}}$	0.255	-0.256	0.141	-0.485
Welch P_{total}	0.254	0.177	0.124	0.062
AR(16) P_{LF}	0.760	0.416	0.339	0.245
AR(16) P_{HF}	0.763	0.992	0.377	0.718
AR(16) $P_{\text{LF}}/P_{\text{HF}}$	0.008	-0.538	-0.026	-0.434
AR(16) P_{total}	0.720	0.408	0.322	0.168

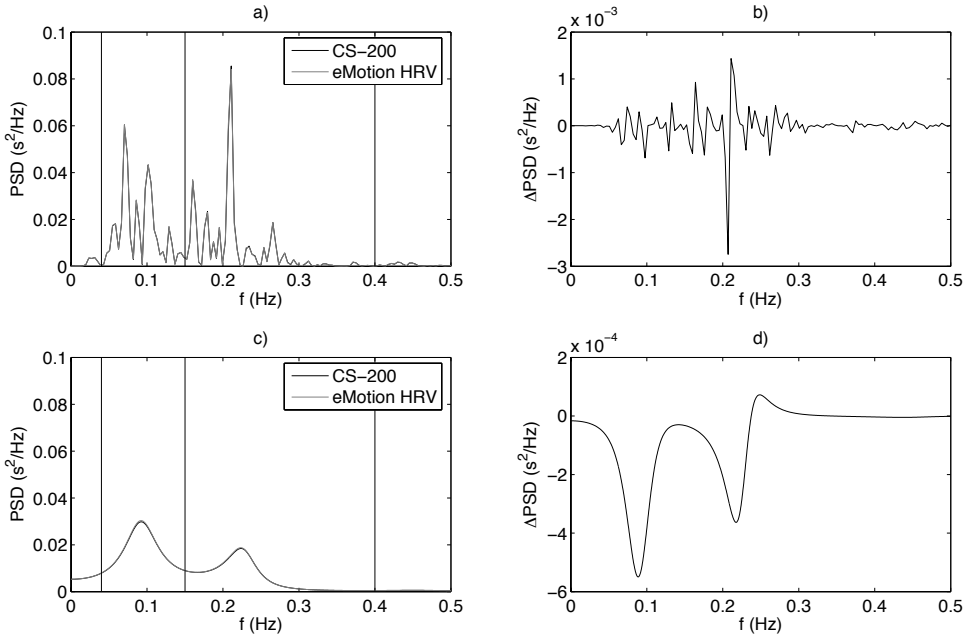

Figure 7.8: The spectrum estimates and differences of spectrum estimates for the standing phase of the orthostatic experiment. a) Welch's periodogram, spectrum estimates from both systems. b) Welch's periodogram, difference between systems. c) AR(16), spectrum estimates from both systems. d) AR(16), difference between systems.

7.4 Long-term Daily Activity Experiment

The 24 hour long daily activity measurements were analysed visually and the artefacts in the signal were detected with the median filtering algorithm. The length of the measurements was less than 24 hours in two cases because of an electrode tearing off during the night and due to taking a shower. The ratio of artefacts for each measurement is presented in Table 7.6. Figure 7.9 shows two examples of the daily activity HRV measurement and the detected artefacts with activity notes made by the subjects, while the Figure 7.10 shows a part of the first measurement with the detected artefacts to demonstrate the performance of the artefact detection algorithm.

Activities that caused artefacts to the measured HRV time series included disrobing a jacket, bicycling, weight lifting, cleaning, embarking and disembarking a truck, playing badminton and running. Also, occasional missed or spurious beats during normal life were detected. On the other hand, activities during which no artefacts were present included driving a truck, playing guitar, stepper training, lower body muscle training and bicycling.

The ratios of artefacts are generally low, but differ multifold between subjects. This fact, together with occurrence of measurement artefacts during light activity, such as sitting, suggest that the placement of the electrodes failed for the subject number two and three. Activities generally causing more artefacts to the measurement, especially with these two subjects, were associated with activity of upper body muscles, while activities with active lower body muscles resulted in good signal quality. EMG of the pectoralis muscles therefore seems to cause artefacts in the measurement. Nevertheless, the low artefact ratios prove the applicability of the eMotion HRV system for long-term ambulatory measurements in normal daily activity with correct electrode placement.

Table 7.6: Number and ratio of artefacts in the daily activity measurements.

Subject	$N_{artefacts}$	$N_{artefacts}/N_{all}$ (%)
1	42	0.040
2	273	0.266
3	61	0.111
4	10	0.009
5	75	0.077

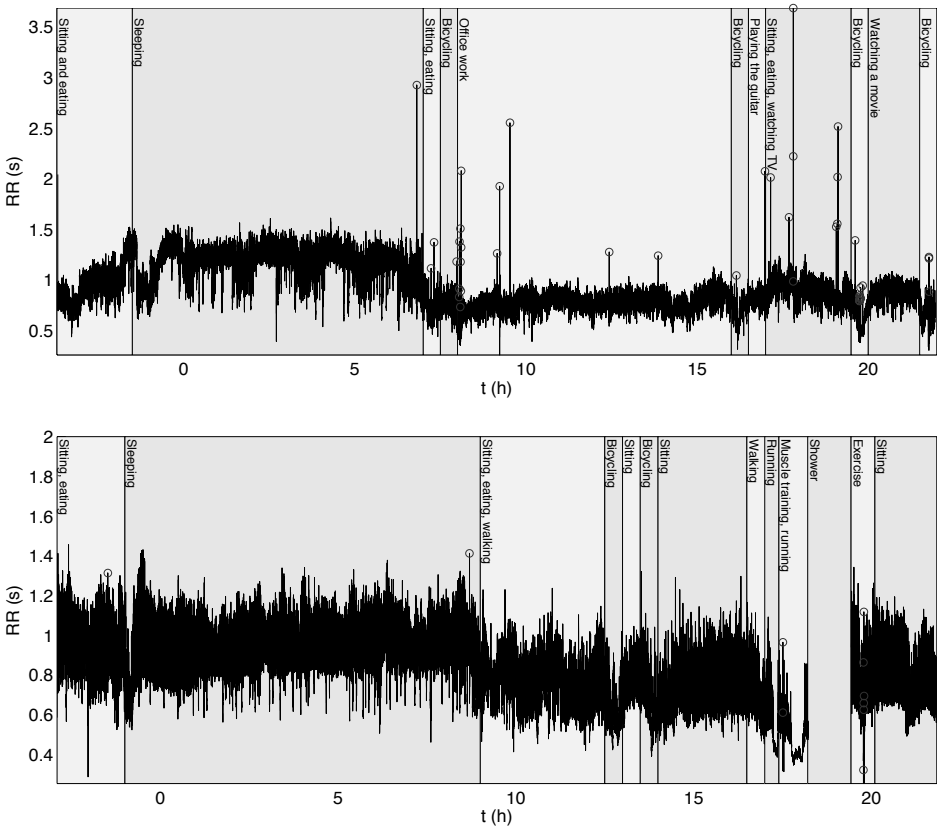

Figure 7.9: Two examples of daily activity HRV measurement. The upper graph is subject 1 and the lower subject is number 4. The activity notes made by the subjects are listed and detected artefacts are shown with (o).

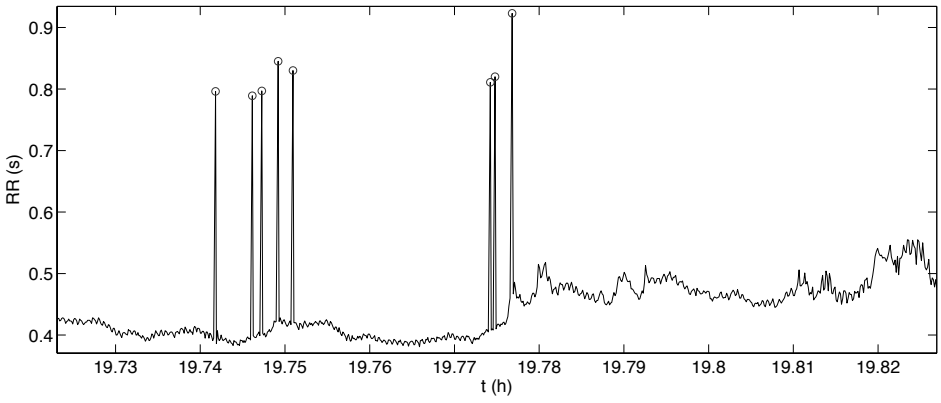

Figure 7.10: An example of performance of the artefact detection algorithm on the 24 hour daily activity measurements. The detected artefacts are shown with (o).

Chapter 8

Conclusions

In this thesis, the eMotion HRV measurement system was introduced and validated. In addition, the development of the data acquisition software for the system was described. To justify the methods of validation, theory on the physiological origin of HRV as well as measurement and analysis methods of HRV were discussed.

The objectives of the validation were 1) to assess the accuracy of the eMotion HRV QRS detector with sensitivity and positive predictivity measures, 2) to analyse the absolute beat-to-beat differences between eMotion HRV and the comparison system data with histogram and Bland-Altman analysis, 3) to analyse the relative differences in HRV measures calculated from the data of the two systems, 4) to assess the quality of long-term measurements conducted with the eMotion HRV system and to identify possible sources of measurement artefact during normal daily activity.

The measures weighing the accuracy of the QRS detection capability of the system were high ($s_{\mathrm{qrs}} = 99.989\,\%$, $p_{\mathrm{qrs}} = 99.989\,\%$) in the orthostatic and exercise experiments. The results of the histogram and Bland-Altman analysis, on the other hand, confirmed that the eMotion HRV system is also precise (0.591 ± 0.962 ms during rest and 0.820 ± 1.308 ms during exercise) in the measurement of RR intervals, which can be over ten times more precise as chest strap measurements [44].

The effect of the differences in RR values between systems on HRV measures was assessed by calculating several well known HRV measures for both systems in the orthostatic experiment. The calculated measures were time domain measures $\overline{\mathrm{RR}}$, $\overline{\mathrm{HR}}$, SDNN and RMSSD and frequency domain measures P_{LF}, P_{HF}, $P_{\mathrm{LF}}/P_{\mathrm{HF}}$ and P_{total} using the spectrum estimation methods Welch's periodogram and stationary AR(16) model. The population average of relative differences of the measures between systems was 0.001 % at the lowest and 0.718 % at the highest, further proving the preciseness of the eMotion HRV system.

The artefact ratios in the long-term daily activity experiment were small: 0.009 % at the lowest and 0.266 % at the highest. The low ratios prove the applicability of the eMotion HRV system for long-term measurements in normal daily activity.

There is a need for accurate, precise, and reliable HRV measurement systems, which are yet unobtrusive and simple to use. All in all, the results of the validation experiments show that the system fulfills these needs for ambulatory measurements in resting as well as in exercise conditions.

[1] Acharya UA, Joseph KP, Kannathal N, Choo Min Lim & Suri JS. Heart rate variability: a review. *Medical and Biological Engineering and Computing*, 44:1031–1051, 2006.

[2] Akaike H. Fitting Autoregressive Models for Prediction. *Annals of the Institute of Statistical Mathematics*, 21(1):243–247, 1969.

[3] Altman DG & Bland JM. Measurement in Medicine: the Analysis of Method Comparison Studies. *The Statistician*, 32:307–317, 1983.

[4] Berntson GG & Stowell JR. Ecg artifacts and heart period variability: Don't miss a beat! *Psychophysiology*, 35:127–132, 1998.

[5] Berntson GG, Bigger JT JR, Eckberg DL, Grossman P, Kaufmann PG, Malik M, Nagaraja HN, Porges SW, Saul JP, Stone PH & Van der Molen MW. Committee Report. Heart Rate Variability: Origins, Methods and Interpretive Caveats. *Psychophysiology*, 34:623–648, 1997.

[6] Boulton JM, Vinik AI, Arezzo JC, Bril V, Feldman EL, Freeman R, Malik RA, Maser RE, Sosenko JM & Ziegler D. Diabetic Neuropathies: A Statement by the American Diabetes Association. *Diabetes Care*, 28:956–962, 2005.

[7] Christov II. Real Time Electrocardiogram QRS Detector Using Combined Adaptive Threshold. *Biomedical Engineering Online*, 3(28), 2004.

[8] Cygankiewicz I, Zareba W & de Luna AB. Prognostic Value of Holter Monitoring in Congestive Heart Failure. *Cardiology Journal*, 15:313–323, 2008.

[9] Einthoven W. *Galvanometrische registratie van het menschelijk electrocardiogram*, pages 101–106. Herinneringsbundel Rosenstein SS, 1902.

[10] Gladwell VF, Fletcher J, Patel N, Elvidge LJ, Lloyd D, Chowdhary S & Coote JH. The influence of small fibre muscle mechanoreceptors on the cardiac vagus in humans. *Journal of Physiology*, 567:713–721, 2005.

[11] Gustafsson F & Hjalmarsson H. Twenty-one ML Estimators for Model Selection. *Automatica*, 22(10):1377–1392, 1995.

[12] Heikkilä J, Kupari M, Airaksinen J, Huikuri H, Nieminen MS & Peuhkurinen K. *Kardiologia, 2nd Edition.* Duodecim, Jyväskylä, Finland, 2008.

[13] Heikkilä J, Mäkijärvi M. *EKG.* Duodecim, Hämeenlinna, Finland, 2003.

[14] Hermens HJ et al. *European Recommendations for Surface ElectroMyoGraphy.* Roessingh Research and Development b.v., 1999.

[15] International Organization for Standardization. *Standard ISO/IEC 23270:2006(E): Information technology - Programming languages - C#.* ISO copyright office, Switzerland, 2006.

[16] Karjalainen PA. *Data Analysis.* University of Kuopio Department of Physics Report Series, ISSN 0788-4672, Kuopio, Finland, 2008.

[17] Kligfield P, Gettes LS, Bailey JJ, Childers R, Deal BJ, Hancock EW, van Herpen G, Kors JA, Macfarlane P, Mirvis DM, Pahlm O, Rautaharju P & Wagner GS. Recommendations for the Standardization and Interpretation of the Electrocardiogram. Part I: The Electrocardiogram and Its Technology. A Scientific Statement From the American Heart Association Electrocardiography and Arrhythmias Committee, Council on Clinical Cardiology; the American College of Cardiology Foundation; and the Heart Rhythm Society. *Journal of the American College of Cardiology*, 49(10):1109–1127, 2007.

[18] Köhler B-U, Hennig C & Orglmeister R. QRS Detection Using Zero Crossing Counts. *Journal of Clinical Monitoring and Computing*, 8(3):138–145, 2003.

[19] Levkov C, Mihov G, Ivanov R, Daskalov D, Christov I & Dotsinsky I. Removal of power-line interference from the ECG: a review of the subtraction procedure. *BioMedical Engineering OnLine*, 4:50, 2005.

[20] Liao D, Barnes RW, Chambless LE & Heiss G. A computer algorithm to impute interrupted heart rate data for the spectral analysis of heart rate variability - the ARIC study. *Computers and Biomedical Research*, 29(2):140–151, 1996.

[21] Malik M, Farrel T, Cribbs T & Camm AJ. Heart rate variability in relation to prognosis after myocardial infarction: selection of optimal processing techniques. *European Heart Journal*, 10:1060–1074, 1989.

[22] Malmivuo J & Plonsey R. *Bioelectromagnetism - Principles and Applications of Bioelectric and Biomagnetic Fields.* Oxford University Press, New York, USA, 1995.

[23] Marple SL Jr. *Digital Spectral Analysis with Applications.* Martin Marietta Aerospace, Baltimore, USA, 1987.

[24] Mason RE & Likar I. A new system of multiple-lead exercise electrocardiography. *Americal Heart Journal*, 71(2):196–205, 1966.

[25] Merri M, Farden DC, Mottley JG & Titlebaum EL. Sampling Frequency of the Electrocardiogram for Spectral Analysis of the Heart Rate Variability. *IEEE Transactions on Biomedical Engineering*, 37(1):99–106, 1990.

[26] Montgomery PG, Green DJ, Etxebarria N, Pyne DB, Saunders PU, & Minahan CL. Validation of Heart Rate Monitor Based Predictions of Oxygen Uptake and Energy Expenditure. *Journal of Strength and Conditioning Research*, 23(5):1489–1495, 2009.

[27] Nagae D & Mase A. Measurement of heart rate variability and stress evaluation by using microwave reflectometric vital signal sensing. *Review of Scientific Instruments*, 81:094301, 2010.

[28] Niskanen JP, Tarvainen MP, Ranta-Aho PO & Karjalainen PA. Software for advanced HRV analysis. *Computer Methods and Programs Biomedicine*, 76(1):73–81, 2004.

[29] Pan J & Tompkins W. A Real-Time QRS Detection Algorithm. *IEEE Transactions on Biomedical Engineering*, BME-32:230–236, 1985.

[30] Portet F, Hernández & Carrault G. Evaluation of Real-Time QRS Detection Algorithms in Variable Contexts. *Medical & Biological Engineering & Computing*, 43:379–385, 2005.

[31] Rand J, Hoover A, Fishel S, Moss J, Pappas J & Muth E. Real-Time Correction of Heart Beat Intervals. *IEEE Transactions on Biomedical Engineering*, 54(5):946–950, 2007.

[32] Rangayyan RM. *Biomedical Signal Analysis: A Case-Study Approach*. IEEE Press, Wiley-Interscience, New York, USA, 2002.

[33] Riniolo T & Porges SW. Inferential and descriptive influences on measures of respiratory sinus arrhythmia: Sampling rate, r-wave trigger accuracy, and variance estimates. *Psychophysiology*, 24(5):613–621, 1997.

[34] Rissanen J. A Universal Prior for Integers and Estimation by Minimum Description Length. *The Annals of Statistics*, 11(2):416–431, 1983.

[35] Schijvenaars BJA, van Herpen G & Kors JA. Intraindividual variability in electrocardiograms. *Journal of Electrocardiology*, 41:190–196, 2008.

[36] Tarvainen MP. *Estimation Methods for Nonstationary Biosignals*. PhD thesis, University of Kuopio, Kuopio, Finland, 2004.

[37] Tarvainen MP, Ranta-aho PO & Karjalainen PA. An advanced detrending method with application to HRV analysis. *IEEE Transactions of Biomedical Engineering*, 49(2):172–175, 2001.

[38] Task Force of the European Society of Cardiology and the North American Society of Pacing and Electrophysiology. Standards of measurement, physiological interpretation, and clinical use. *European Heart Journal*, 17:354–381, 1996.

[39] Thakor NV, Webster JG & Tompkins WJ. Estimation of QRS Complex Power Spectra for Design of a QRS Filter. *IEEE Transactions on Biomedical Engineering*, 31(11):702–706, 1984.

[40] Van Leeuwen P. Fetal Magnetocardiography: Time Intervals and Heart Rate Variability. *Neurology and Clinical Neurophysiology*, 46, 2004.

[41] Verklan MT, Padhye NS & Brazdeikis A. Analysis of Fetal Heart Rate Variability Obtained by Magnetocardiography. *Journal of Perinatal & Newnatal Nursing*, 20:343–348, 2006.

[42] Webster JG. *Medical Instrumentation: Application and Design.* Houghton Mifflin, Boston, USA, 1992.

[43] Weimer LH. Autonomic Testing - Common Techniques and Clinical Applications. *The Neurologist*, 16:215–222, 2010.

[44] Weippert M, Kumar M, Kreuzfeld S, Arndt D, Rieger A & Stoll R. Comparison of three mobile devices for measuring R-R intervals and heart rate variability: Polar S810i, Suunto t6 and an ambulatory ECG system. *European Journal of Applied Physiology*, 109:779–786, 2010.

[45] Welch PD. Use of fast Fourier transform for estimation of power spectra - a method based on time averaging over short modified periodograms. *IEEE Transactions on Audio and Electroacoustics*, AU-15:70–73, 1967.